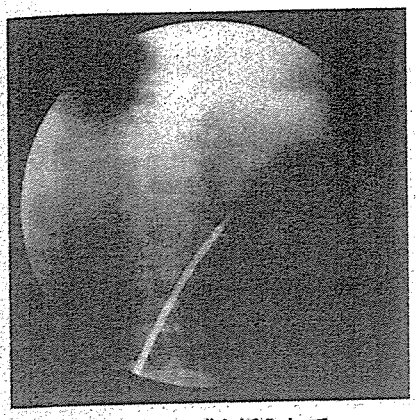

図8 胃瘻チューブを挿入してパラシュートを開き固定

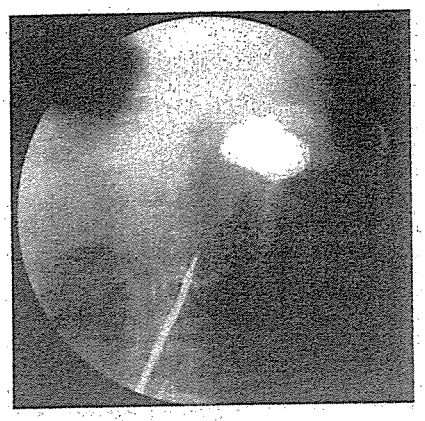

図9 造影による確認

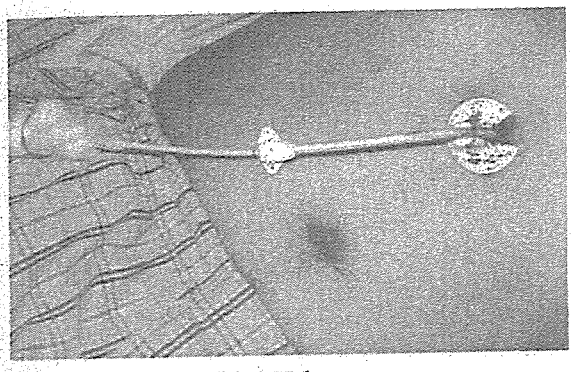

図10 胃瘻チューブ皮膚固定

7) 16Fピールアウェイシース挿入 (図7)

16Fピールアウェイシースは胃瘻チューブをより確実に挿入するために用いている。抜去は，胃瘻チューブ挿入完了後に，胃瘻チューブが抜けないように注意深く行う。

8) 胃瘻チューブ挿入と固定 (図8～10)

ピールアウェイシースのなかを通して挿入し，チューブを安定した形にする。確認造影した後，固定し手技終了となる。アンカーは胃瘻チューブに固定しておき，3日目に問題がないことを確認後，切断している。

結　果

44例中41例 (93%) で成功し，不成功に終わった3例中2例では再施行で成功している。不成功となった3例は，空気の胃壁内注入で胃内腔の拡張ができなかったこと，アンカーが手技中に切れチューブ挿入が困難となったこと，およびルート拡張中にダイレータが胃壁外へ逸脱したことがその原因であった。不成功のうちで，空気の胃壁内注入で胃内腔の拡張ができなかった症例では，その後，経過中に全身状態の悪化があり，再施行を断念した。全例で手技に伴う重篤な合併症はみとめなかった。

◎

CT-PGは，頭頸部悪性腫瘍による消化管閉塞症例に対し有用で，開腹的胃瘻造設術に代わりうる方法と考えられる。IVR CTアンギオシステムを用いると，患者を寝台移動させることなく，円滑かつ迅速にCT透視下からX線透視下に移動できることより，CT-PGばかりでなく，他のCTガイド下IVRに有用である。しかし，CT透視下で行うものとX線透視下で可能なものに手技を分けて工夫することで，細心の注意を要するが，IVR CTアンギオシステムのない施設でも十分施行可能であると考える。

CTガイド下IVRには，その他の領域においても大きな可能性がある。しかし一方で，今後解決されるべき被曝の問題があるのも現実である。X線ビーム内では，通常CT透視で用いられる80kV，30mAの条件で，等価線量率は1.47±0.03mSv/secである。これに両手の年間等価線量率の上限が500mSvであることを考慮すると，年被曝時間の上限は340秒である。徒手によるCT透視断面へ穿刺針を整合させるのは熟練を要し，標的病変に穿刺を的中させる時間を加算すると，術者のX線被曝の問題は無視できないものになる。

献身的な姿勢は大切であるが，X線ビームから4cmの位置では等価線量率は0.025±0.001mSv/secとなり，年被曝時間の上限も20000秒に延長することなども考慮し，術者は，技術の鍛錬とともに，放射線防護に気を配らなければならない。

穿刺針の確実なCT透視断面への整合性を有し，かつ術者被曝軽減を兼ね備えたCT透視専用の穿刺装置の開発が待望される。

●参考文献
1) 佐竹光夫：IVR CT/angio system. 腹部血管造影ハンドブック，大友　邦 編，東京，中外医学社，132～157，1999.
2) 林　信成：経皮的胃十二指腸瘻造設術. 臨床放射線，34，395～398，1989.
3) 高村和人・他：経皮内視鏡的胃瘻造設術において横行結腸穿孔を来した1例. 広島医学，53・8，769～771，2000.
4) Kanazawa, S., et al.: Percutaneous feeding gastrostomy in patients with a partial gastrectomy ; Transhepatic approach with CT guidance. *Abdom. Imaging*, **20**, 302～306, 1995.
5) Hawkins, I.F. : Carbon dioxide subtraction arteriography. *AJR*, **139**, 19～24, 1982.
6) Halkier, B.K., et al.: Percutaneous feeding gastrostomy with the Seldinger technique ; Review of 252 patients. *Radiology*, **171**, 71～74, 1985.

Am J Clin Oncol (CCT) 26(2): 159–164. 2003.

Pilot Study of Transcatheter Arterial Chemoembolization with Degradable Starch Microspheres in Patients With Hepatocellular Carcinoma

Junji Furuse, M.D., Hiroshi Ishii, M.D., Mitsuo Satake, M.D., Hiroaki Onaya, M.D., Haruhiko Nose, M.D., Shigeru Mikami, M.D., Hideki Sakai, M.D., Kiyomi Mera, M.D., Yasushi Maru, M.D., and Masahiro Yoshino, M.D.

We prospectively evaluated the efficacy and safety of transcatheter arterial chemoembolization (TACE) with microembolization material, degradable starch microspheres (DSMs), and epirubicin, for treatment of multifocal hepatocellular carcinoma (HCC). Seventeen patients with multifocal HCC were treated. At the first treatment, DSMs were injected alone to determine the dose for embolization of the hepatic artery in each patient. After 4 weeks, TACE was performed every 4 to 6 weeks with a mixture of DSMs and epirubicin at a dose of 40 mg/m^2. A necrotic area of more than 50% was produced in 6 patients by DSMs alone, and in 11 patients by TACE. The overall response rate was 52.9% (2 complete and 7 partial responses). The duration of the responses ranged from 4 to 21 months (median: 9 months). Common toxicities were transient abdominal pain, nausea/vomiting, fever, and leukopenia. In four patients, grade III or IV toxicity was observed as γ-glutamyl transpeptidase elevation. TACE with DSMs had tumor necrosis efficacy with acceptable toxicity. The median survival time was 21.7 months, and the 2-year survival rate was 45.3%. Further investigation of the effects of DSM treatment on survival should be carried out.
Key Words: Hepatocellular carcinoma—Degradable starch microsphere—Transcatheter arterial chemoembolization.

Percutaneous ethanol injection or thermal ablation therapy, including microwave coagulation therapy and radiofrequency, are considered the most effective nonsurgical therapeutic approaches of choice for treatment of hepatocellular carcinoma (HCC).[1–4] However, these therapeutic methods are generally indicated for patients with earlier stage HCC, and there are many patients with advanced HCC who are not eligible for these treatments because of the multifocality of the tumor. Transcatheter arterial embolization (TAE) with gelatin sponge particles has been effectively applied to patients with advanced HCC, because HCCs receive a rich blood supply, mainly through the hepatic artery.[5] Furthermore, TAE combined with iodized oil and anticancer drugs—transcatheter arterial chemoembolization (TACE)—has improved the HCC anticancer efficacy, by inducing extensive tumor necrosis and improved survival.[6–9] Nevertheless, several controlled trials did not demonstrate any significant benefit of TAE on survival.[10–13] Several factors may account for these poor results. Although TAE has to be performed repeatedly to obtain more extensive necrosis in patients with multifocal tumors, it could be argued that Gelfoam will provide a more proximal obstruction and that proximal obstruction could enhance the development of blood supply coming from phrenic or omental arteries, or aberrant collaterals.[12] Furthermore, patients with cirrhosis and HCC frequently die of liver failure.[11,14–16]

Degradable starch microspheres (DSM) were developed to provide transient occlusion of small arteries.[17,18] The microspheres are $45 \pm 7 \times 10^{-6}$ m in diameter and descend to the arteriole/capillary level, where they lodge.[19] The duration of occlusion in the hepatic arteries by DSM is limited to 80 minutes.[20] An anticancer drug coadministered with DSM is selectively trapped with DSM in small arteries, and is concentrated in areas of liver tumor. Consequently, the activity of the drug is expected to increase.[19,21] Several studies in metastatic liver tumors indicate that intraarterial therapy with DSM and anticancer drug improved the therapeutic effects, compared with an anticancer drug alone.[20,22–24] HCC has

Division of Hepatobiliary Pancreatic Medical Oncology (J.F., H.I., K.M., Y.M., M.Y.) and Department of Radiology (M.S., H.O.), National Cancer Center Hospital East; Department of Internal Medicine, Chiba Social Insurance Hospital (H.I., Y.M.); Department of Internal Medicine, Chiba Rosai Hospital (H.N.); Department of Internal Medicine, Kikkoman General Hospital (S.M.); Department of Internal Medicine, Kashiwa City Hospital (H.S.), Chiba, Japan.

Supported by Grants-in-Aid for Cancer Research and the Second Term Comprehensive 10-year Strategy for Cancer Control grant from the Ministry of Health and Welfare of Japan.

Address correspondence and reprint requests to Dr. Junji Furuse, National Cancer Center Hospital East, 6-5-1, Kashiwanoha, Kashiwa, Chiba 277-8577, Japan. E-mail: jfuruse@east.ncc.go.jp

a rich blood supply from hepatic arteries and DSM is expected to be even more useful in the treatment of HCC than for liver metastatic tumors. In patients with advanced HCC, Carr et al.[25] reported a high response rate (63%) in a phase II study of DSM injected in the hepatic artery in conjunction with doxorubicin and cisplatin. However, no studies to date have investigated transcatheter arterial treatment using DSM alone or combination DSM and epirubicin in patients with advanced HCC. We therefore conducted a preliminary prospective study of transcatheter arterial treatment using DSM and epirubicin to clarify the efficacy and safety of this treatment. The primary endpoint was antitumor effect and the secondary endpoints were adverse effects of this treatment and survival.

MATERIALS AND METHODS

The eligibility criteria for enrolling in the study were 1) a diagnosis of HCC based on histologic findings or findings of cirrhosis due to type B or C hepatitis virus, liver tumor with tumor staining by hepatic angiography, and a serum α-fetoprotein value exceeding 250 ng/ml; 2) no indication of hepatic resection, percutaneous ethanol injection, or thermal ablation therapy; 3) no portal vein tumor thrombus in main portal vein; 4) bidimensionally measurable hepatic lesions; 5) age 15 to 75 years; 6) no treatment of HCC for 3 months before this treatment; 7) a performance status of 0, 1, or 2 based on the Eastern Cooperative Oncology Group score; 8) an anticipated life expectancy of at least 3 months; 9) adequate renal function (serum creatinine concentration <1.1 mg/dl, blood urea nitrogen level <22 mg/dl), and adequate hepatic function (serum bilirubin level <3.0 mg/dl, serum alanine and aspartate transaminase levels less than 5 times the upper normal limits), adequate bone marrow function (leukocyte count >3,000 cells/mm^3, platelet count >50,000 cells/mm^3, and hemoglobin >7.5 g/dl); 10) written informed consent provided by the patient; and 11) feasibility of angiography and catheter introduction in hepatic arteries. Patients were excluded from the study if they had active peptic ulcer, uncontrollable ascites or pleural effusion, uncontrollable hepatic encephalopathy, or any other preexisting medical condition of sufficient severity to prevent full compliance with the study. The study protocol was approved by an institutional review board of our institution.

The femoral artery was catheterized while patients were under local anesthesia. To obtain information about hepatic arteries, tumors, tumor thrombi, and portal hemodynamics before embolization, digital subtraction angiography was performed selectively in the celiac and proper, right, or left hepatic artery, and portography was performed from the superior mesenteric artery. The tip of the catheter was placed in the proper hepatic artery or right and/or left hepatic artery to inject embolic agents. At the first treatment, DSM was administered alone to ascertain the optimal DSM dosage per patient for subsequent treatments with combination DSM and epirubicin. DSM, at a concentration of 300 mg per 3 ml of contrast medium, was injected until embolization of peripheral hepatic arteries was confirmed (Fig. 1A,B). Four weeks after the treatment with DSM alone, TACE with a mixture of DSM and epirubicin at a dose of 40 mg/m^2 was performed; the latter was repeated every 4 to 6 weeks until there was evidence of disease progression or unacceptable toxicity. To adjust the DSM dose to the condition of the hepatic artery at each treatment, the mixture of epirubicin and about 80% dosage of the optimal DSM was administered, and then the remainder of DSM was administered until the hepatic artery was embolized.

Patients were evaluated for response according to the standard World Health Organization criteria.[26] The antitumor response was assessed by dynamic computed tomography (CT), at the early phase, at 7 days, and at 4 weeks after the administration of DSM alone, and 4 weeks after every TACE with DSM and epirubicin. The hypoattenuated area was evaluated as tumor necrosis area without contrast enhancement at the early phase of dynamic CT. Toxic effects were evaluated using the National Cancer Institute common toxicity criteria[27], and survival was calculated from the date of the administration of DSM alone using the Kaplan-Meier method.

Standard statistical methods and a two-stage design were used in this protocol.[28] We expected a more than 40% response rate in this treatment, because the response rate was about 40% in repeated arterial infusion chemotherapy with an anticancer drug and Lipiodol.[29] If only 3 complete (CR) or partial responses (PR) were noted in the first 17 patients, a response rate of more than 40% could be excluded with 95% confidence and accrual would stop. Therefore, we set 17 evaluable patients as the number of patients in this pilot study.

RESULTS

Patients

Eighteen patients were enrolled in this study between February and August 1999. The patient characteristics are shown in Table 1. In one patient, hepatic arterial flow was not static even with 1,500 mg of DSM and the artery could not be embolized. This patient was excluded from the following TACE with DSM and epirubicin and the analysis. The efficacy and toxicity of this treatment were evaluable in the other 17 patients. Eleven patients had histologically confirmed HCC and the other six were diagnosed based on clinical findings. Follow-up continued between 4.4 and 29.0 months from the beginning of this treatment.

Treatments

At the first administration of DSM, the average dose, which embolized the hepatic artery, was 920 mg (range, 300–1,800 mg) in 17 patients. The 17 patients received a total of 66 courses of this procedure (mean, 3.9 courses; range, 2–7 courses). The mean cumulative dose of DSM was 3,097 mg (range, 600–8,400 mg). The mean cumulative dose of epirubicin was 166 mg/body (range, 60–250 mg/body). Treatment was discontinued in all 17 patients. The reasons for the discontinuation were due to progression of the disease, after evaluation of CR, PR, and no change (NC) in 14 patients, narrowing of hepatic artery in 1, and patient refusal of this treatment in 2. With regard to treatments after discontinuance of this study, the patient with narrowing of hepatic artery and 2 patients with refusal of the treatment in this study received supportive care after then. Three of the 14 patients with progression of the disease had local regrowth in 2 or 3 HCC lesions and therefore underwent ablation therapy by percutaneous ethanol injection or microwave coagu-

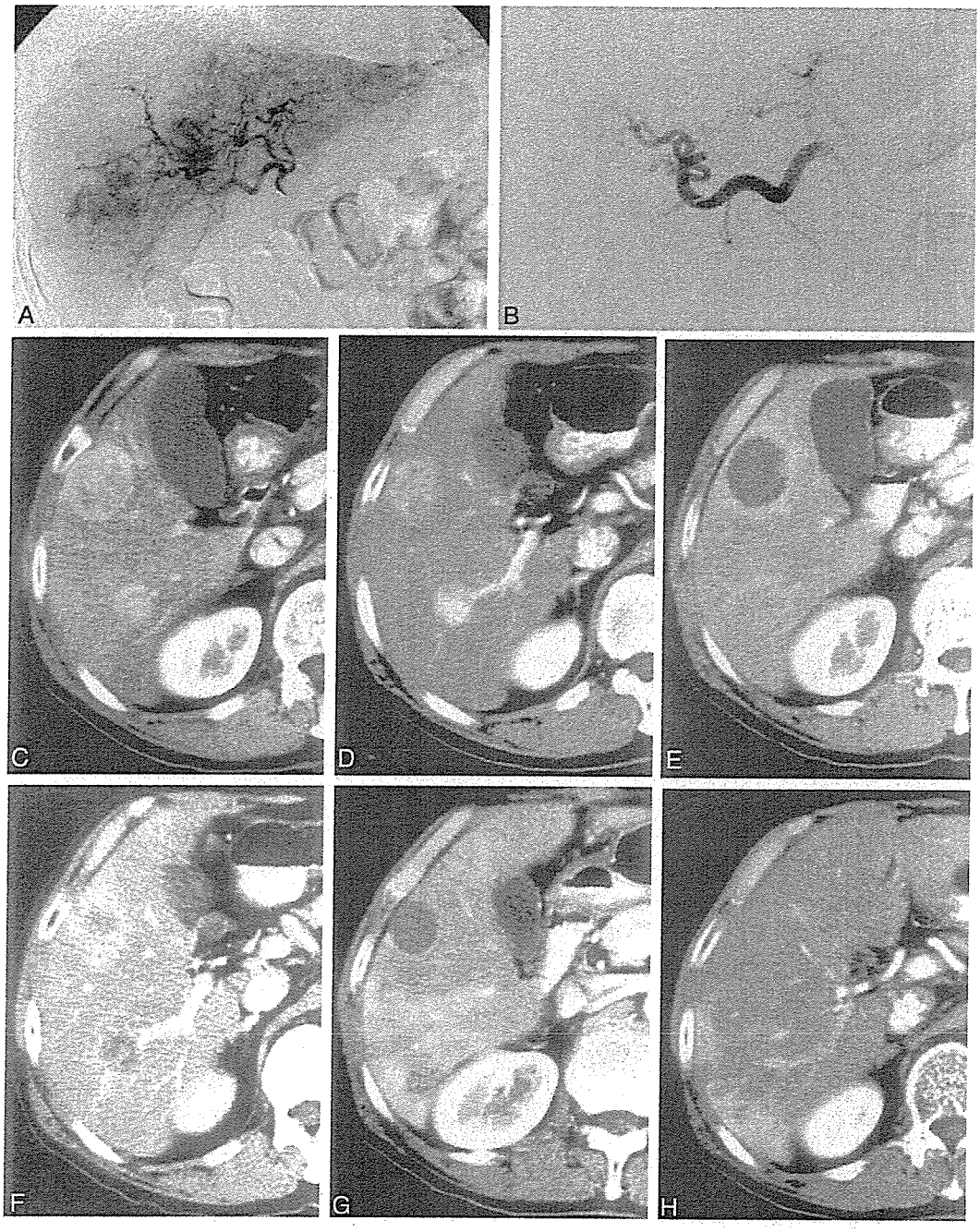

FIG. 1. Sixty-two-year-old man with multiple tumors of hepatocellular carcinoma (HCC). **A.** Hepatic angiogram shows staining of multiple tumors, which are diagnosed as HCC. **B.** Hepatic angiogram after degradable starch microspheres (DSM) injection. The main branches of the hepatic artery are embolized. **C, D.** The early phase of dynamic computed tomography (CT) before injection of DSM alone shows high-attenuation areas in the right lobe of the liver (arrow). **E, F.** The early phase of dynamic CT 7 days after DSM injection. A whole tumor at the anterior inferior segment of the liver changed to a hypoattenuated area and a ring-enhanced lesion is observed around the tumor. Another tumor at the posterior inferior segment partially changed to a hypoattenuated area. These hypoattenuated areas indicate DSM-induced necrosis. **G, H.** The early phase of dynamic CT 5 months after injection of DSM alone and transcatheter arterial chemoembolization with a mixture of DSM and epirubicin at the same level of the liver. A tumor at the anterior inferior segment is still a hypoattenuated area and the other is observed as partially hypoattenuated. The response to treatment was evaluated as partial in this patient.

TABLE 1. *Patient characteristics*

Variable	No. of patients (n = 18)
Sex (M/F)	15/3
Age (y)*	64 ± 5
Performance status† (0/1)	17/1
Viral markers	
HBs Ag(+), HCV Ab(−)	1
HBs Ag(−), HCV Ab(+)	14
HBs Ag(−), HCV Ab(−)	3
Child-Pugh classification A/B/C	12/4/2
Previous treatment	
Transcatheter arterial embolization and/or percutaneous ethanol injection	7
None	11
Tumor location Unilateral lobe/bilateral lobe	2/16
Number of tumors 4/5/>5	4/2/12
Size of largest tumor (cm) ≤ 3/>3, ≤5/>5	11/3/4
Alpha-fetoprotein (ng/ml) ≤20/>20, ≤100/>100	5/5/8

* Data expressed as mean ± SD.
† Eastern Cooperative Oncology Group score: 0 (fully active), 1 (restricted in physically strenuous activity), 2 (ambulatory and fully capable of self-care), 3 (capable of only limited self-care), and 4 (completely disabled).

lation therapy for the viable tumors. Eight of the 14 patients received conventional TACE with a mixture of iodized oil and epirubicin followed by gelatin sponge particles, because they still had more than three viable lesions and had never undergone the conventional TACE before. The remaining three patients received supportive care because of hepatic failure[2] and refusal of treatment.[1]

Response

Tumor necrosis of more than 50% was obtained by the embolization with DSM alone in 6 of 17 patients (35.3%) (Fig. 1C–F). In the evaluation of TACE with DSM and epirubicin, two patients (11.8%) had achieved a CR, and 7 (41.2%) a PR (Fig. 1G,H). The overall response rate (CR and PR) was 52.9% (95% CI, 31.0–73.8%). The duration of the responses ranged from 4 to 21 months (median, 9 months). Of the remaining 8 patients, 7 were NC (41.2%) and 1 progressive disease (PD) (5.9%). Tumor necrosis of more than 50% was obtained in the 11 patients (64.7; 95% CI, 41.3–82.6%), including total tumor necrosis in 4 (23.5%), a CR in 2 and a PR in 2.

Toxicity

Treatment-related toxicities are summarized in Table 2. Nausea, abdominal pain, fever, and leukopenia were the most common types of toxicity, but they were limited within grade II. Nausea and abdominal pain were observed within 1 hour after the treatment in most patients. Abdominal pain was usually relieved completely by administration of nonsteroidal antiinflammatory drugs,

TABLE 2. *Maximum treatment-associated toxicities*

Toxicity	No. of patients (n = 18)	Grade I	II	III	IV
Abdominal pain	8 (44.4%)	5	3	0	0
Nausea	8 (44.4%)	7	1	0	0
Vomiting	4 (22.2%)	4	0	0	0
Fever	8 (44.4%)	4	4	0	0
Leukopenia	8 (44.4%)	5	3	0	0
g-GTP	5 (27.8%)	0	1	3	1
Alp	3 (16.7%)	3	0	0	0
SGOT, SGPT	0	0	0	0	0
Erythema	1 (5.6%)	1	0	0	0
Cholecystitis	1 (5.6%)	1	0	0	0
Ascites	1 (5.6%)	0	1	0	0

Alp, alkaline phosphatase; g-GTP, gamma-glutamyl transpeptidase; SGOT, serum glutamic oxaloacetic transaminase; SGPT, serum glutamic pyruvic transaminase.

and seven patients needed narcotic analgesics. Fever was self-limited, lasting less than 5 days. Treatment was not discontinued because of these toxicities. The only grade III or IV toxicity was elevation of serum γ-glutamyl transpeptidase (GTP) in 4 patients (22.2%), grade III in 3 patients, and grade IV in 1. Grade I or II elevation of serum alkaline phosphatase was also observed in such patients. However, they were resolved by administration of urodesoxycholic acid.

Survival

Survival curves are shown in Figure 2. Of the 17 patients, 7 died of tumor progression, 2 died of hepatic failure, and 1 died of respiratory failure due to chronic pulmonary emphysema and pneumonia. The median survival time was 21.7 months, and the 1- and 2-year survival rates were 64.7% and 45.3%, respectively.

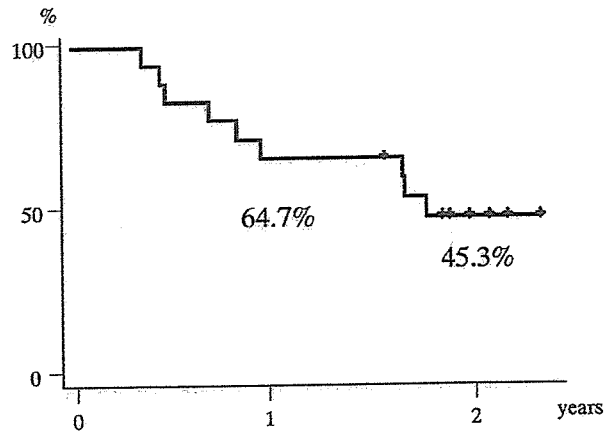

FIG. 2. Survival for patients treated by transcatheter arterial chemoembolization with a mixture of degradable starch microspheres and epirubicin.

DISCUSSION

Gelatin sponge particles are generally used as embolization material in TAE for HCC. In a phase II study, Bruix et al.[30] reported a favorable response (extensive necrosis with reduction of tumor area greater than 50%) in 81% of patients by TAE with small cubes of gelatin and steel coils, but without intraarterial chemotherapy. DSMs were developed to provide transient occlusion of small arteries. However, no published studies have yet reported the embolization effect of DSM for HCC. In this study, the necrotic area induced by the hepatic arterial occlusion using DSM alone varied from 0% to 80%, and a favorable response of tumor necrosis greater than 50% was seen in 35.3% of evaluable patients. These results confirmed that DSMs itself had varying degrees of antitumor effect against HCC, despite the fact that embolization was only temporary.

In hepatic metastases, tumor uptake of anticancer drug can be increased by hepatic arterial infusion with DSM, and combined anticancer drug with DSM has been recommended as intraarterial infusion therapy.[20,22–24] In this pilot study, we performed TACE using a mixture of DSM and anticancer drug for advanced HCC. We used epirubicin as the anticancer drug, because it was reported to have a superior therapeutic effect by intraarterial administration for HCC.[31] A favorable response of tumor necrosis greater than 50% was observed in 64.7% patients by TACE, including complete necrosis in 23.5% of patients. This result was much greater than that of DSM alone.

Although the chemoembolization by gelatin and anticancer drug is widely used, severe complications have been reported. A randomized trial in France indicated that liver failure occurred in 30 of 50 patients assigned to chemoembolization.[11] It was reported that the hepatic dysfunction had often worsened, with jaundice, ascites, and/or hepatic encephalopathy after chemoembolization.[8,9] The mortality rate within the first 60 days after TAE using gelatin was reported to range from 7% to 17%.[9,32–34] In contrast, a series of this treatment with DSM did not induce severe liver dysfunction, and there was no early mortality. Abdominal pain immediately after the treatment tended to be severe in some patients, but fever and abdominal pain throughout this treatment seemed to be less than with TAE with gelatin. The only grade III or IV toxicity was elevation of γ-GTP, which is characteristic of this treatment. Elevation of serum alkaline phosphatase was also observed in such patients. However, there were no accompanying symptoms. We speculated that peripheral cholangitis occurred because of peripheral hepatic artery occlusion by DSM.

It is not clear whether TAE can prolong survival in patients with advanced HCC. Several randomized trials have shown that TAE had a marked antitumor effect, but it did not definitely improve the survival.[10–13] One reason for this discrepancy is deterioration of liver function due to treatment, and there is a need for development of a treatment method with fewer side effects. Our study of TACE with DSM and epirubicin to reduce adverse effects on liver function shows favorable antitumor effect and fewer adverse effects. However, the duration of the responses was limited, and 14 of 17 patients abandoned treatment because of disease progression. The 2-year survival rates in this study were similar to reports of TACE randomized controlled trials, with 2-year survival rate of approximately 40%.[10–13] Our results do not confirm whether TACE using DSM can improve the survival in patients with advanced HCC. Phase II or III studies involving a larger number of patients should be conducted to determine effects of DSM treatment on survival.

REFERENCES

1. Livraghi T, Festi D, Monti F, et al. US-guided percutaneous alcohol injection of small hepatic and abdominal tumors. *Radiology* 1986;161:309–312.
2. Ebara M, Ohto M, Sugiura N, Kita K, et al. Percutaneous ethanol injection for the treatment of small hepatocellular carcinoma. Study of 95 patients. *J Gastroenterol Hepatol* 1990;5:616–626.
3. Seki T, Wakabayashi M, Nakagawa T, et al. Ultrasonically guided percutaneous microwave coagulation therapy for small hepatocellular carcinoma. *Cancer* 1994;74:817–825.
4. Rossi S, Di Stasi M, Buscarini E, et al. Percutaneous RF interstitial thermal ablation in the treatment of hepatic cancer. *AJR* 1996;167: 759–768.
5. Matsui O, Kadoya M, Kameyama T, et al. Benign and malignant nodules in cirrhotic livers: distinction based on blood supply. *Radiology* 1991;178:493–497.
6. Yamada R, Sato M, Kawabata M, et al. Hepatic artery embolization in 120 patients with unresectable hepatoma. *Radiology* 1983; 148:397–401.
7. Kasugai H, Kojima J, Tatsuta M, et al. Treatment of hepatocellular carcinoma by transcatheter arterial embolization combined with intraarterial infusion of a mixture of cisplatin and ethiodized oil. *Gastroenterology* 1989;97:965–971.
8. Venook AP, Stagg RJ, Lewis BJ, et al. Chemoembolization for hepatocellular carcinoma. *J Clin Oncol* 1990;8:1108–1114.
9. Vetter D, Wenger JJ, Bergier JM, et al. Transcatheter oily chemoembolization in the management of advanced hepatocellular carcinoma in cirrhosis: results of a Western comparative study in 60 patients. *Hepatology* 1991;13:427–433.
10. Pelletier G, Roche A, Ink O, et al. A randomized trial of hepatic arterial chemoembolization in patients with unresectable hepatocellular carcinoma. *J Hepatology* 1990;11:181–184.
11. Groupe d'Etude et de Traitement du Carcinome Hepatocellulaire. A comparison of lipiodol chemoembolization and conservative treatment for unresectable hepatocellular carcinoma. *N Engl J Med* 1995;332:1256–1261.
12. Bruix J, Llovet JM, Castells A, et al. Transcatheter arterial embolization versus symptomatic treatment in patients with advanced hepatocellular carcinoma: results of a randomized, controlled trial in a single institution. *Hepatology* 1998;27:1578–1583.
13. Pelletier G, Ducreux M, Gay F, et al. Treatment of unresectable hepatocellular carcinoma with lipiodol chemoembolization: a multicenter randomized trial. Groupe CHC. *J Hepatol* 1998;29:129–134.
14. Okuda K, Ohtsuki T, Obata H, et al. Natural history of hepatocellular carcinoma and prognosis in relation to treatment. Study of 850 patients. *Cancer* 1985;56:918–928.
15. Calvet X, Bruix J, Bru C, et al. Natural history of hepatocellular carcinoma in Spain. Five years' experience in 249 cases. *J Hepatol* 1990;10:311–317.
16. The Liver Cancer Study Group of Japan. Primary liver cancer in Japan: clinicopathologic features and results of surgical treatments. *Ann Surg* 1990;211:277–287.

17. Forsberg JO. Transient blood flow reduction induced by intra-arterial injection of degradable starch microspheres. Experiments on rats. *Acta Chir Scand* 1978;144:275–281.
18. Lindell B, Aronsen KF, Rothman U. Repeated arterial embolization of rat livers by degradable microspheres. *Eur Surg Res* 1977;9:347–356.
19. Sigurdson ER, Ridge JA, Daly JM. Intra-arterial infusion of doxorubicin with degradable starch microspheres. Improvement of hepatic tumor drug uptake. *Arch Surg* 1986;121:1277–1281.
20. Dakhil S, Ensminger W, Cho K, et al. Improved regional selectivity of hepatic arterial BCNU with degradable microspheres. *Cancer* 1982;50:631–635.
21. Aronsen KF, Hellekant C, Holmberg J, et al. Controlled blocking of hepatic artery flow with enzymatically degradable microspheres combined with oncolytic drugs. *Eur Surg Res* 1979;11:99–106.
22. Ensminger WD, Gyves JW, Stetson P, et al. Phase I study of hepatic arterial degradable starch microspheres and mitomycin. *Cancer Res* 1985;45:4464–4467.
23. Taguchi T, Tanikawa K, Sano K, et al. Multi-center cooperative phase II study of combined infusion of PJ-203 (degradable starch microspheres) into hepatic artery in metastatic liver cancer [in Japanese]. *Gan To Kagaku Ryoho* 1993;20:2015–2025.
24. Taguchi T. Chemo-occlusion for the treatment of liver cancer. A new technique using degradable starch microspheres. *Clin Pharmacokinet* 1994;26:275–291.
25. Carr BI, Zajko A, Bron K, et al. Phase II study of Spherex (degradable starch microspheres) injected into the hepatic artery in conjunction with doxorubicin and cisplatin in the treatment of advanced-stage hepatocellular carcinoma: interim analysis. *Semin Oncol* 1997;24(suppl 6):97–99.
26. World Health Organization. *WHO handbook for reporting results of cancer treatment: Offset publication 48.* Geneva: World Health Organization, 1979.
27. Ajani JA, Welch SR, Raber MN, et al. Comprehensive criteria for assessing therapy-induced toxicity. *Cancer Invest* 1990;8:147–159.
28. Simon R. How large should a phase II trial of a new drug be? *Cancer Treat Rep* 1987;71:1079–1085.
29. Minoyama A, Yoshikawa M, Ebara M, et al. Study of repeated arterial infusion chemotherapy with a subcutaneously implanted reservoir for advanced hepatocellular carcinoma. *J Gastroenterol* 1995;30:356–366.
30. Bruix J, Castells A, Montanya X, et al. Phase II study of transcatheter arterial embolization in European patients with hepatocellular carcinoma: need for controlled trials. *Hepatology* 1994;20:643–650.
31. Epirubicin Study Group for Hepatocellular Carcinoma. Intra-arterial administration of epirubicin in the treatment of nonresectable hepatocellular carcinoma. *Cancer Chemother Pharmacol* 1987;19:183–9.
32. Taniguchi K, Nakata K, Kato Y, et al. Treatment of hepatocellular carcinoma with transcatheter arterial embolization. Analysis of prognostic factors. *Cancer* 1994;73:1341–1345.
33. Bismuth H, Morino M, Sherlock D, et al. Primary treatment of hepatocellular carcinoma by arterial chemoembolization. *Am J Surg* 1992;163:387–394.
34. Stuart K, Stokes K, Jenkins R, et al. Treatment of hepatocellular carcinoma using doxorubicin/ethiodized S oil/gelatin powder chemoembolization. *Cancer* 1993;72:3202–3209.

Gastrointestinal Stromal Tumor

Correlation of Computed Tomography Findings with Tumor Grade and Mortality

Ukihide Tateishi, MD, PhD, Tadashi Hasegawa, MD, PhD, Mitsuo Satake, MD, and Noriyuki Moriyama, MD, PhD

Objectives: To assess computed tomography (CT) findings to assist in the distinction of low- and high-grade gastrointestinal stromal tumors (GISTs) and to estimate their relative risk (RR) for mortality.

Methods: Sixty-nine patients with clinicopathologically and immunohistochemically proven GISTs, including 44 patients with low-grade tumors and 25 with high-grade tumors, who underwent dual-phase CT for initial examination were included. Images were assessed retrospectively for tumor size, location, epicenter, types of surface, boundary, presence of invasion, enhancement pattern, hepatic metastasis, and peritoneal dissemination. Their RR for mortality was estimated by using a multiple logistic regression model.

Results: Statistically significant CT findings favoring a diagnosis of high-grade GIST and affecting the 5-year survival rate included a lesion larger than 11.1 cm (median + 1 SD), irregular surface, unclear boundary, presence of invasion, heterogeneous enhancement, hepatic metastasis, and peritoneal dissemination. Multivariate analysis showed RRs for mortality in lesions larger than 11.1 cm (RR = 3.9), with the presence of wall invasion (RR = 5.1), and with hepatic metastasis (RR = 11.3), respectively.

Conclusions: The CT features that suggest a high-grade GIST and predict poor outcome include hepatic metastasis, presence of wall invasion, and lesions larger than 11.1 cm.

Key Words: gastrointestinal stromal tumor, prognosis, computed tomography

(*J Comput Assist Tomogr* 2003;27:792–798)

From the Divisions of Diagnostic Radiology (Drs Tateishi and Moriyama) and Pathology (Dr Hasegawa), National Cancer Center Hospital and Institute, Tokyo, Japan.

Reprints: Dr. U. Tateishi, Division of Diagnostic Radiology, National Cancer Center Hospital, 5-1-1, Tsukiji, Chuo-Ku, 104–0045, Tokyo, Japan (e-mail: utateish@ncc.go.jp).

This work was supported in part by grants from Scientific Research Expenses for Health and Welfare Programs, The Foundation for the Promotion of Cancer Research, and Second-Term Comprehensive 10-Year Strategy for Cancer Control.

A gastrointestinal stromal tumor (GIST) is defined as a mesenchymal tumor of the gastrointestinal (GI) tract that expresses consistent immunoreactivity for CD117, a c-kit proto-oncogene protein.[1–4] Gastrointestinal stromal tumors have a wide clinical spectrum ranging from low- to high-grade tumors, and their differentiation and biologic behavior are continuing topics of controversy. The term *gastrointestinal stromal tumor* has been used to refer to the main group of mesenchymal tumors of the GI tract, which included leiomyoma, leiomyosarcoma, leiomyoblastoma, schwannoma, glomus tumor, neurofibroma, and ganglioneuroma. Recent advances in our understanding of molecular pathogenesis may have significant clinical importance, however, making it necessary to define and diagnose such tumors accurately.[5–9] The term *gastrointestinal stromal tumor* should be reserved for a more specific group of tumors than previously were included. For the purpose of our review, we have clearly distinguished between GISTs and other mesenchymal tumors arising in the GI tract. This definition especially excludes GI true smooth muscle tumors and neurogenic tumors that do not express CD117. The definite identification of GISTs has become increasingly important, because a Kit-selective tyrosine kinase inhibitor, imatinib mesylate (Gleevec, formerly known as STI571; Novartis, East Hanover, NJ), has shown promise as an effective adjuvant therapy treatment.[8,9]

As for the biologic behavior of a GIST, tumor size, mitotic rate, tumor necrosis, and Ki-67 (MIB-1, a 395-kd nuclear antigen) index have been associated with malignancy and accepted as important prognostic factors to estimate the risk of metastasis and mortality by means of recent pathologic studies.[10,11]

The computed tomography (CT) and magnetic resonance imaging features of GI stromal sarcoma have been reported previously.[12–19] Few articles have described the distinction of low- and high-grade tumors on the basis of pathologic definition, however, and with an emphasis on prognosis. In this study, the dual-phase CT features of 69 patients with pathologically confirmed GISTs at a single institution with a long follow-up period were investigated retrospectively for

distinction of low- and high-grade tumors based on the definite histopathologic grading system, and the effect of CT findings on prognosis was estimated by multivariate analysis.

MATERIALS AND METHODS

Patients

We reviewed 69 patients with primary GISTs who were registered in the pathology files. The clinical details, including follow-up information, were obtained by reviewing all medical charts. No patients were lost to follow-up. Follow-up began on the date of primary surgery. Overall survival was recorded as the time to death as a result of any cause.

Pathologic Review

Histologic slides of all patients were reviewed for diagnosis by an expert pathologist who had developed the grading system (MIB-1 system). Immunohistochemistry was performed by the labeled streptavidin–biotin method, with appropriate use of positive and negative controls. The primary antibodies used in the present study were CD117 (c-kit, polyclonal, 1:50, autoclave; Dako) and Ki-67 (MIB-1, 1:100, autoclave; Dako). Ki-67 (MIB-1 index) was estimated by counting the percentage of positive cell nuclei per 1000 tumor cells in the region of the tumor with the greatest density of staining. In the present study, the histologic grading was determined by a 3-grade system.[3] By this histologic grading system, 44 tumors (63.8%) were classified as low grade and 25 tumors (36.2%) were classified as high grade.

Dual-Phase CT Scan

The dual-phase CT imaging was performed before surgery with 1 of 2 scanners in all patients (Aquilion multislice CT scanner [n = 22] or X-Vigor helical CT scanner [n = 47]; both from Toshiba Medical Systems, Tokyo, Japan). Patients were examined while in the supine position and received iodinated nonionic contrast material (300 mgI/mL) intravenously at a rate of 3.0 mL/s for a total of 100 mL with an autoinjector (Autoenhance A-250 or A-50; Nemoto-kyorindo, Tokyo, Japan). Scans were obtained 30 and 60 seconds after the start of the injection during the arterial dominant and parenchymal phases, respectively, so as to differentiate between inner and outer layers of wall structures in the target organ. Patients also received 300 mL water with a single oral bolus and were rescanned if GI distention was inadequate. Scanning parameters were an axial single-slice or 4-slice mode, 3.0- to 5.0-mm section thickness, 0.5 to 1.0 seconds of rotation, pitch of 1–3, 120 to 150 kV (peak), and 200 to 250 mA. Images were reconstructed with 3.0- (n = 22), 5.0- (n = 26), and 10.0-mm (n = 69) slice thicknesses using a standard algorithm without edge enhancement. These scanning parameters were selected to scan the abdominal region as rapidly as possible without impairing image quality. All helical scans were obtained at the top of the liver in a cephalocaudal direction.

TABLE 1. Patient Demographics and Lesion Location

Demographic	Low-Grade Tumor (n = 44)	High-Grade Tumor (n = 25)	*P* Value*
Gender			
Male	26	13	0.57
Female	18	12	
Age (yr)			
Mean	68.9	65.1	0.21
Median	70.5	67.0	
Range	47–87	35–80	
Lesion Location			0.03†
Upper location	38	16	
Esophagus	0	1	
Stomach	38	15	
Lower location	6	9	
Small intestine	4	6	
Rectum	2	3	

*Gender was compared by using the χ^2 test. Age was compared by using the Wilcoxon rank sum test. Lesion location was compared by using the fisher exact test.

†*P* value for upper versus lower location.

Imaging and Histopathologic Analyses

Two board-certified radiologists retrospectively reviewed the CT images, and the findings were reported as a consensus opinion without knowledge of the pathologic subtype or tumor grade of the GISTs. All images were interpreted using hard copy films. Lesions were judged by tumor size, lo-

TABLE 2. Odds Ratios for Computed Tomography Findings Favoring a Diagnosis of High-Grade Gastrointestinal Stromal Tumor

CT Findings	Odds Ratio	95% CI
Size ≥11.1 cm (vs. size <11.1 cm)	322.7	31.7–3281.3
Extrinsic epicenter (vs. intrinsic epicenter)	17.9	9.3–34.4
Irregular surface (vs. regular surface)	19.4	3.8–98.0
Unclear boundary (vs. clear boundary)	22.8	4.5–115.2
Invasion of mesentery (vs. absent)	9.1	1.7–48.1
Wall invasion (vs. absent)	16.5	3.3–82.3
Heterogeneous enhancement (vs. homogeneous enhancement)	13.5	4.0–44.9

95% CI indicates 95% confidence interval; CT, computed tomography.

cation, epicenter (intrinsic or extrinsic), type of surface (regular or irregular), boundary (clear or unclear), internal architecture, presence of invasion (mesentery or wall of target organ), hepatic metastasis, and peritoneal dissemination. Both the inner and outer layers of the wall were determined by CT images of the arterial dominant and parenchymal phases. The presence of wall invasion was defined as a lesion involving more than 50% of the entire wall or a lesion without distinction between the inner and outer layers of thickened wall. The contrast enhancement patterns were recorded as homogeneous or heterogeneous. The degree of enhancement was graded as follows: marked, or tumor attenuation higher than that of the liver; moderate, or tumor attenuation between that of the liver and that of muscle; and low, or tumor attenuation lower than that of muscle. Other associated findings such as calcification were also evaluated. The histopathologic findings in surgical specimens from all the patients were retrospectively reviewed by the pathologist, with special emphasis on tumor invasion. One radiologist and 1 pathologist correlated the CT findings with the histopathologic findings by means of a layer-to-layer comparison.

Statistical Analysis

Patient demographics and imaging characteristics were compared by using the χ^2 test, Fisher exact test probability test, or Wilcoxon rank sum test for categorized variables. Univariate analysis was performed by comparing Kaplan-Meyer survival curves and log rank tests. The relative risk (RR) of each

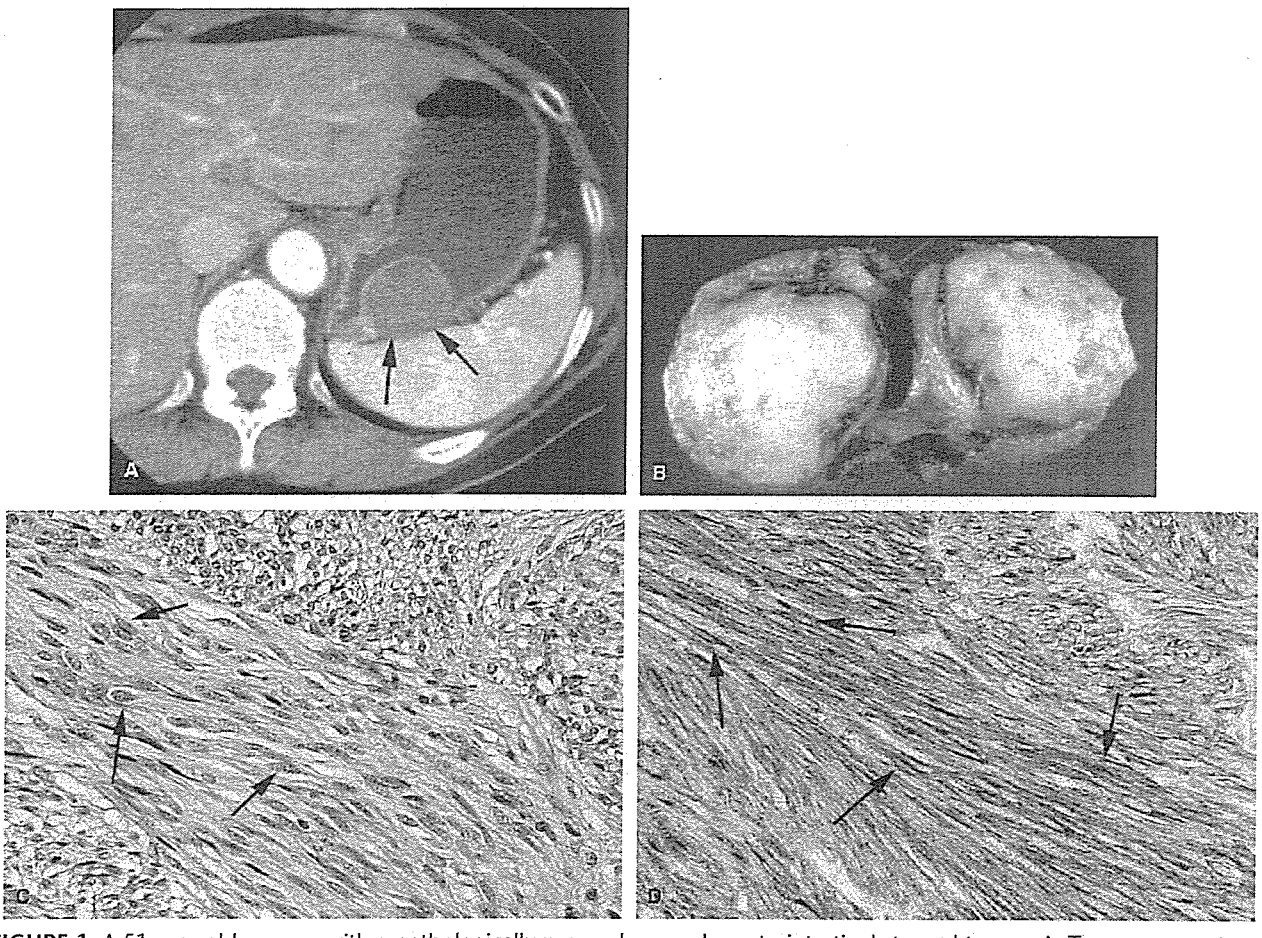

FIGURE 1. A 51-year-old woman with a pathologically proven low-grade gastrointestinal stromal tumor. A, Transverse contrast-enhanced computed tomography scan obtained in arterial dominant phase demonstrates a hypoattenuating mass compared with the hyperattenuating inner layer of stomach. Tumor exhibits regular surface and intrinsic epicenter. Tumor is seen to arise from submucosal layer of fundus (arrows). B, Photograph of gross pathologic specimen shows localized tumor without invasion. C, Photomicrograph of histologic specimen (hematoxylin–eosin stain, original magnification 100×) demonstrates cellular fascicles of spindle tumor cells with few mitotic figures. D, Photomicrograph of histologic specimen (CD117 immunohistochemical stain, original magnification 100×) shows diffuse and strong staining for CD117.

variable was estimated by a Cox proportional hazards model in multivariate analysis. Multivariate analysis was conducted with variable selection by both a stepwise forward procedure and backward elimination. All analyses were conducted using SPSS software (version 11.0J; SPSS, Chicago, IL). A P value of 0.05 was considered to indicate a statistically significant difference.

RESULTS

Clinical Characteristics

Patient demographics and lesion location are shown in Table 1. Comparison of the age and sex distribution of patients with low-grade tumors versus high-grade tumors was not statistically significant. Of 69 patients with GISTs, 39 were male (56.5%) and 30 were female (43.5%). The mean age at the time of presentation was 67 years (range: 35–87 years), and 32 patients (46.4%) were less than 67 years of age. Presenting symptoms were more often found in patients with high-grade tumors (51.9%) than in those with low-grade tumors (26.2%). The most common symptoms were pain in 17 patients (24.6%), followed by masses in 5 (7.2%), GI bleeding in 3 (4.3%), and signs of obstruction in 3 (4.3%). High-grade tumors were significantly more common in the small intestine and rectum than in the esophagus and stomach ($P = 0.03$). Fifty-three tumors (76.8%) occurred in the stomach, 10 tumors (14.5%) occurred in the small intestine, 5 tumors (7.2%) occurred in the rectum, and 1 tumor (1.5%) occurred in the esophagus.

CT Findings

Our comparison of the CT findings is illustrated in Table 2. The mean tumor size was 5.4 cm (SD = 5.7 cm, range: 1.0–38.0 cm), and 23 tumors (33.3%) measured greater than 5.4 cm. The mean largest dimension of high-grade tumors was greater than that of low-grade tumors. The epicenter of the tumor was identified as intrinsic in 38 tumors (55.1%) and extrinsic in 31 tumors (44.9%). Twenty-one tumors (91.3%) with extrinsic epicenters were larger than the mean tumor size. Fifty-five tumors (79.7%) had a regular surface (Fig. 1). The mass was regarded as focal and the boundary was clear in 54 patients (78.3%). Mesenteric invasion (Fig. 2) as evidenced by soft tissue stranding of mesentery or surrounding fat was present in 13 patients (18.8%). All tumors were seen with a low attenuating compared with high-attenuating inner layer in the arterial dominant phase. Twenty-three tumors (33.3%) showed heterogeneous enhancement in the parenchymal phase, suggesting the presence of necrosis, degeneration, or hemorrhage. Seventeen tumors (74.0%) with heterogeneous enhancement were greater than the mean tumor size. Heterogeneous enhancement was a significant predictor of high-grade tumor. Discernible soft tissue masses involved more than 50% of the entire wall of the target organ in 8 patients (11.6%). Lesions without distinction between the inner and outer layers of thickened wall were seen in 13 patients (18.8%). Ulceration (Fig. 3) and cystic formation (Fig. 4), respectively, were seen in 2 high-grade tumors (2.9%). In 1 patient (1.4%), mild enlargement of the gastric wall with discernible cystic masses was seen on CT (see Fig. 4). Hepatic metastases were identified in 11 patients (15.9%). The frequency of hepatic metastasis was statistically greater in high-grade tumors than in low-grade tumors ($P < 0.001$). The mean size of tumors associated with hepatic metastasis was 8.8 cm in diameter (range: 2–17 cm). Peritoneal dissemination was found in 9 patients with high-grade tumors, whereas none was found in patients with low-grade tumors ($P < 0.001$). Punctate calcification (Fig. 5) was noted in 7 cases (10.1%). Punctate calcification was seen in 3 low-grade tumors and in 4 high-grade tumors, which was not statistically significant. Additional CT findings, including limited mesenteric lymphadenopathy, were not seen in any patients. Statistically significant CT findings of high-grade tumors included an extrinsic epicenter, irregular surface, unclear boundary, mesenteric invasion, wall invasion, and heterogeneous enhancement pattern ($P < 0.001$). The odds ratios (ie, that CT features favoring a diagnosis of high-grade GIST) are shown in Table 2. By using a final multiple stepwise logistic regression model, an extrinsic epicenter (RR = 8.5, 95% confidence interval [CI]: 2.0–35.4) and unclear boundary (RR = 6.5, 95% CI: 1.1–38.6) were the most significant predictors of high-grade GIST.

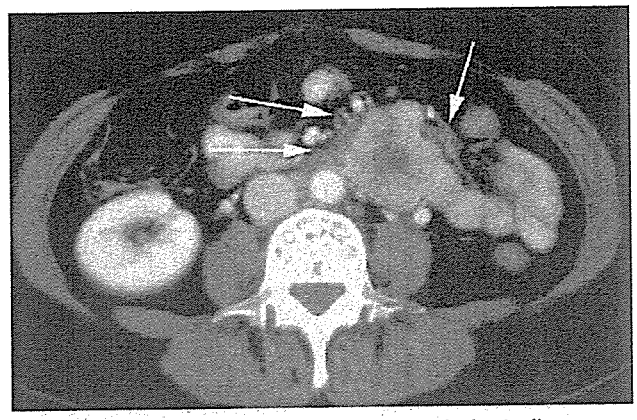

FIGURE 2. A 58-year-old woman with a pathologically proven high-grade gastrointestinal stromal tumor. Transverse contrast-enhanced computed tomography scan shows mesenteric invasion (arrows) of tumor arising from the duodenum.

Prognostic Analysis

At the latest follow-up, in which the mean follow-up period for living patients was 63.7 months, 15 (21.7%) of 69 patients with GISTs had died, giving a 5-year survival rate of 84.3%. In the univariate analysis (Table 3), the features, including tumor size larger than 11.1 cm (mean + 1 SD), irregu-

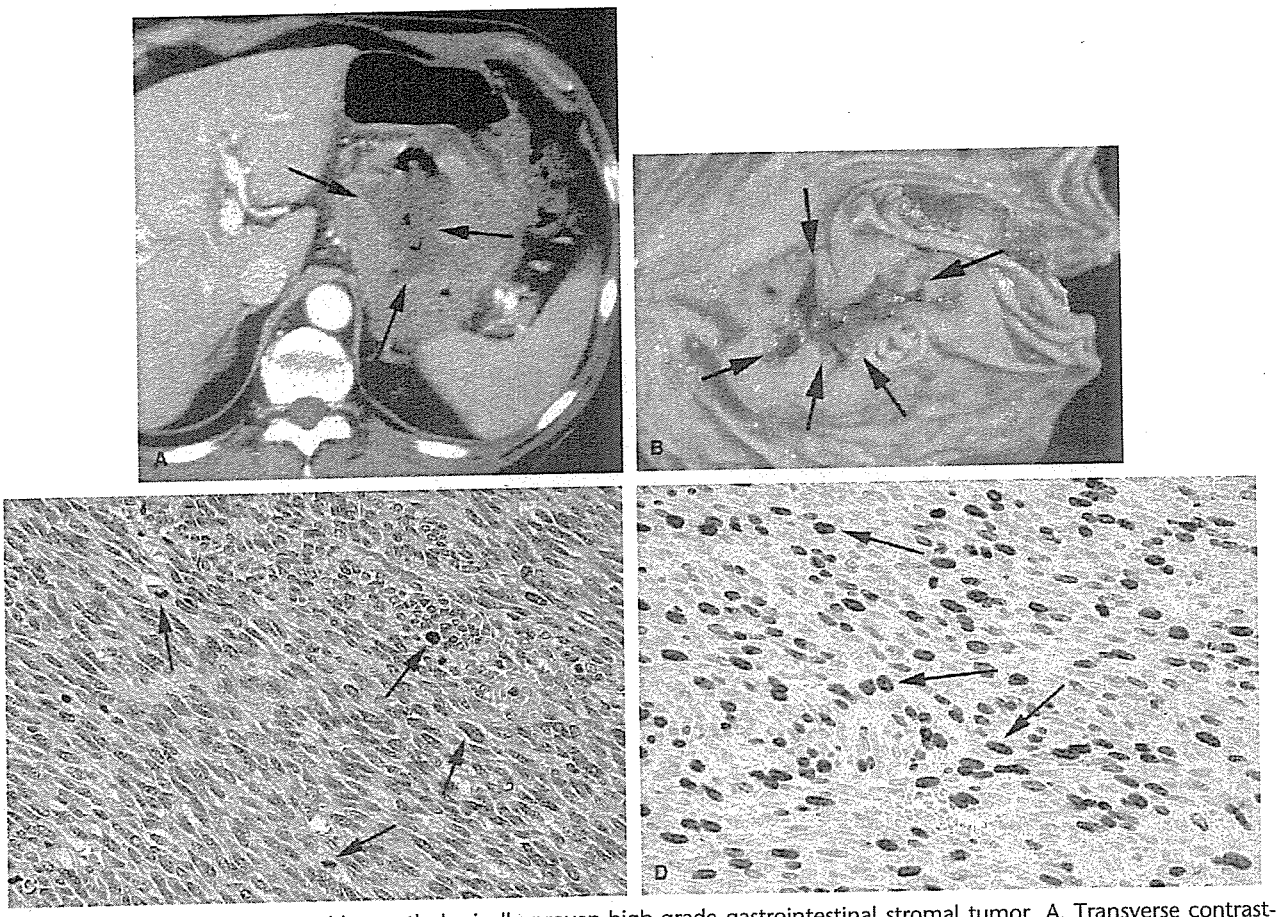

FIGURE 3. A 63-year-old man with a pathologically proven high-grade gastrointestinal stromal tumor. A, Transverse contrast-enhanced computed tomography scan shows a large heterogeneous mass in anterior aspect of stomach. Tumor exhibits extrinsic epicenter and marked ulceration (arrows). B, Photograph of gross pathologic specimen shows ulceration and tumor invasion of mucosal surface (arrows). C, Photomicrograph of histologic specimen (hematoxylin–eosin stain, original magnification 100×) demonstrates marked proliferation of spindle tumor cells with increased mitotic figures. D, Photomicrograph of histologic specimen (MIB-1 immunohistochemical stain, original magnification 100×) shows that an MIB-1 score of 5 is assigned to this tumor based on approximately 50% of cells stained for MIB-1.

lar surface, clear boundary, mesenteric invasion, wall invasion, heterogeneous enhancement, hepatic metastasis, and peritoneal dissemination, had a significant impact on overall survival. In multivariate analysis (Table 4), hepatic metastasis emerged as the most significant adverse prognostic factor, followed by wall invasion and tumor size larger than 11.1 cm.

DISCUSSION

In the current study, we have documented several statistically significant CT features to help distinguish low-grade GISTs from high-grade GISTs, combined with their prognostic value. By using univariate analysis, the CT findings, including lesion larger than 11.1 cm, irregular surface, unclear boundary, presence of invasion, heterogeneous enhancement, hepatic metastasis, and peritoneal dissemination, were more often found in high-grade GISTs and were associated significantly with decreased survival. We also showed that a lesion larger than 11.1 cm, wall invasion of the target organ, and hepatic metastasis identified on CT images had a significant effect on prognosis in multivariate analysis.

Gastrointestinal stromal tumor has become a widely applied term for the specific mesenchymal tumors of the GI tract. Few articles have included a description of imaging findings when using the term *gastrointestinal stromal tumor*, however. A true GIST would be included in the earlier imaging studies of leiomyoma, leiomyoblastoma, or leiomyosarcoma arising in the GI tract. The distribution of high-grade GISTs reviewed in the present study is similar to that reported previously.[5–9] It

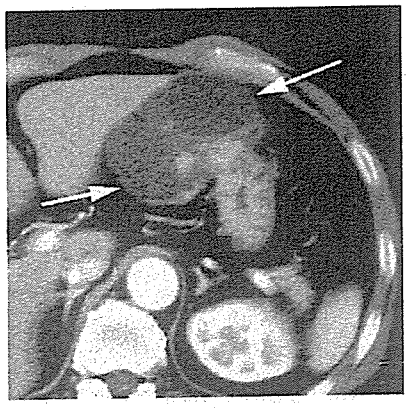

FIGURE 4. A 67-year-old man with a pathologically proven high-grade gastrointestinal stromal tumor. Transverse contrast-enhanced computed tomography scan shows cystic components (arrows) of tumor arising from the stomach.

has been reported that GISTs arising in the small intestine show more malignant behavior than GISTs arising in the stomach.[20] It has also been reported that no significant difference is found in survival curves between stomach and nonstomach sites, however, probably as a result of the small sample size for the latter.

Findings associated with leiomyosarcoma arising in the GI tract include an irregular lobulated mass with low attenuation, central liquefactive necrosis, ulceration, calcification, or direct extension and vascular encasement.[17–19] These are similar to our results, except for a few findings. Calcification is often found in benign stromal tumors of the GI tract.[17] Our results suggested that the frequency of calcification was not a reliable finding for the distinction of low- and high-grade GISTs. Nevertheless, there were too few patients with calcifications to draw a conclusion on its usefulness in the present study. A larger tumor shows an infiltrating mass with no definable shape engulfing multiple segments of the bowel and surrounding mesenteric vessels. Therefore, we assessed mesenteric invasion on dual-phase CT to differentiate between the inner and outer layers of wall structures in the target organ and to differentiate tumor infiltration from vascular structures. As for the enhancement pattern, leiomyoma arising in the GI tract shows a uniform enhancement pattern reaching a peak in the capillary phase on rapid intravenous contrast bolus CT. In contrast to leiomyoma, leiomyosarcoma has been characterized as showing a heterogeneous enhancement pattern, and lesions are composed of a central low-density area and peripheral well-enhanced area.[17] Heterogeneous enhancement was a significant predictor of high-grade tumor but was considered to be a nonspecific finding. The enhancement features of these tumors typically reflect tumor size and tumor outgrowth of blood supply. Large benign leiomyomas may demonstrate heterogeneous enhancement.

Tumor grade has been determined on the basis of the degree of increased cellularity, high nuclear-to-cytoplasmic ratios, and mitotic activity in previous pathologic studies.[8] A poor correlation of cellular atypia with malignant potential on the basis of microscopic observation was found, however. The discrepancy among these results was mainly a result of the

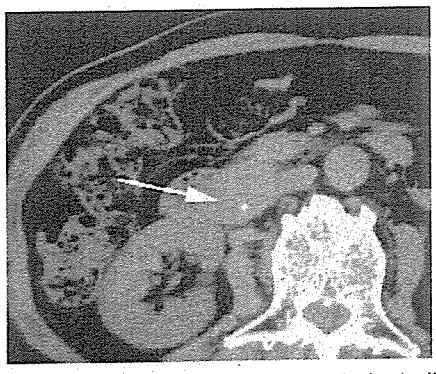

FIGURE 5. A 82-year-old man with a pathologically proven high-grade gastrointestinal stromal tumor. Transverse unenhanced computed tomography scan shows punctate calcification (arrow) of tumor arising from the duodenum.

TABLE 3. Univariate Analysis for Overall Survival in 69 Patients with Gastrointestinal Stromal Tumors

Feature	5-Year Survival Rate	Log Rank *P* Value
Size ≥11.1 cm (vs. size <11.1 cm)	72.9 (89.6)	<0.01
Extrinsic epicenter (vs. intrinsic epicenter)	80.0 (87.8)	0.08
Irregular surface (vs. regular surface)	57.7 (90.8)	<0.01
Unclear boundary (vs. clear boundary)	58.9 (90.7)	<0.01
Invasion of mesentery (vs. absent)	55.0 (90.9)	<0.001
Wall invasion (vs. absent)	55.0 (91.0)	<0.001
Heterogeneous enhancement (vs. homogeneous enhancement)	71.4 (89.7)	<0.05
Hepatic metastasis (vs. absent)	42.4 (91.4)	<0.001
Peritoneal dissemination (vs. absent)	51.9 (89.6)	<0.01

TABLE 4. Multivariate Analysis for Overall Survival in 69 Patients with Gastrointestinal Stromal Tumors*

Variable	Relative Risk	95% CI
Size ≥11.1 cm (vs. size <11.1 cm)	3.9	1.3–11.5
Wall invasion (vs. absent)	5.1	1.8–14.8
Hepatic metastasis (vs. absent)	11.3	2.9–43.3

*Predictors of high-grade tumor selected from features in Table 2, by using stepwise logistic regression.
95% CI indicates 95% confidence interval.

limitation by smaller sample size and differences in the determination of tumor grading. Among the numerous variables responsible for the differences in tumor grading between observers are inaccurate criteria for identifying mitotic figures, quality of tissue processing, and counting area on microscopic observation. MIB-1 is one of the most significant prognostic markers in immunohistochemical analysis. A grading system using MIB-1 scoring was the most significant independent prognostic factor for GISTs.[3] Consequently, we used the MIB-1 score instead of the mitotic score to develop a grading system that proved to be valid and reproducible in the present study. Better pathologic diagnosis and tumor grading are essential components of accurate radiologic-pathologic correlation and treatment decisions.

The overall survival rate of 84.3% after 5 years observed in the current study is higher than those reported in previous studies.[21–24] This may be explained by the large percentage of patients with smaller lesions, which has a significant impact on overall survival figures. A high proportion of smaller tumors arising in the stomach would also have a significant impact on overall survival rates, because these tumors were reported to be associated with relatively higher survival rates after 5 years.[21–24]

Our findings suggest that dual-phase CT is a reliable technique to predict patient prognosis. By using univariate analysis, the CT features, including tumor size (larger than 11.1 cm), irregular surface, clear boundary, mesenteric or wall invasion, heterogeneous enhancement, distant metastasis, and peritoneal dissemination, were significantly associated with poor survival. The present multivariate analysis clearly showed that the CT features, including hepatic metastasis, wall invasion, and large tumor (larger than 11.1 cm), identified on CT were significantly associated with a poor outcome. The evidence of liver metastases evident in our small high-grade lesions indicates that a GIST should be considered potentially malignant and that this prognostic system is useful at the level of individual patients with a GIST. From a clinical standpoint, hepatic metastasis, wall invasion, and large tumor at presentation seem to be fairly sensitive, albeit nonspecific, CT findings for the possibility that a patient may have a high-grade GIST.

The limitation to our study was that ours was a retrospective study in which data were gathered over a period of years, with substantial variations in CT equipment. Nevertheless, given the relatively low frequency of occurrence of GISTs at any single institution, the prospective acquisition of a similar number of cases would require a large multi-institutional study conducted over many years.

In conclusion, we observed statistically significant differences in dual-phase CT findings between patients with low- and high-grade GISTs. Several CT features, including hepatic metastasis, wall invasion, and large tumor size (larger than 11.1 cm), can provide helpful predictive values for a poor outcome.

REFERENCES

1. Miettinen M, Sarlomo-Rikala M, Lasota J. Gastrointestinal stromal tumors: recent advances in understanding of their biology. *Hum Pathol.* 1999;30:1213–1220.
2. Miettinen M, Lasota J. Gastrointestinal stromal tumors—definition, clinical, histopathological, immunohistochemical, and molecular genetic features and differential diagnosis. *Virchows Arch.* 2001;438:1–12.
3. Hasegawa T, Matsuno Y, Shimoda T, et al. Gastrointestinal stromal tumor: consistent CD117 immunostaining for diagnosis, and prognostic classification based on tumor size and MIB-1 grade. *Hum Pathol.* 2002; 33:669–676.
4. Hirota S, Isozaki K, Moriyama Y, et al. Gain-of-function mutations of c-kit in human gastrointestinal stromal tumors. *Science.* 1998;279:577–580.
5. Franquemont DW. Differentiation and risk assessment of gastrointestinal stromal tumors. *Am J Clin Pathol.* 1995;103:41–47.
6. Goldblum JR, Appelman HD. Stromal tumors of the duodenum. A histologic and immunohistochemical study of 20 cases. *Am J Surg Pathol.* 1995;19:71–80.
7. Rudolph P, Gloeckner K, Parwaresch R, et al. Immunophenotype, proliferation, DNA ploidy, and biological behavior of gastrointestinal stromal tumors: a multivariate clinicopathologic study. *Hum Pathol.* 1998;29: 791–800.
8. Dagher R, Cohen M, Williams G, et al. Approval summary: imatinib mesylate in the treatment of metastatic and/or unresectable malignant gastrointestinal stromal tumors. *Clin Cancer Res.* 2002;8:3034–3038.
9. Bauer S, Corless CL, Heinrich MC, et al. Response to imatinib mesylate of a gastrointestinal stromal tumor with very low expression of KIT. *Cancer Chemother Pharmacol.* 2003;51:261–265.
10. Hasegawa T, Yokoyama R, Lee TH, et al. Prognostic relevance of a histological grading system using MIB-1 for adult soft-tissue sarcoma. *Oncology.* 2000;58:66–74.
11. Hasegawa T, Yamamoto S, Nojima T, et al. Validity and reproducibility of histologic diagnosis and grading for adult soft-tissue sarcomas. *Hum Pathol.* 2002;33:111–115.
12. Hasegawa S, Semelka RC, Noone TC, et al. Gastric stromal sarcomas: correlation of MR imaging and histopathologic findings in nine patients. *Radiology.* 1998;208:591–595.
13. Buckley JA, Fishman EK. CT evaluation of small bowel neoplasms: spectrum of disease. *Radiographics.* 1998;18:379–392.
14. Hama Y, Okizuka H, Odajima K, et al. Gastrointestinal stromal tumor of the rectum. *Eur Radiol.* 2001;11:216–219.
15. Shibata Y, Ueda T, Seki H, et al. Gastrointestinal stromal tumor of the rectum. *Eur J Gastroenterol Hepatol.* 2001;13:283–286.
16. Shojaku H, Futasuya R, Seto H, et al. Malignant gastrointestinal stromal tumor of the small intestine: radiologic-pathologic correlation. *Radiat Med.* 1997;15:189–192.
17. Megibow AJ, Balthazar EJ, Hulnick DH, et al. CT evaluation of gastrointestinal leiomyomas and leiomyosarcomas. *AJR Am J Roentgenol.* 1985;144:727–731.
18. McLeod AJ, Zornoza J, Shirkhoda A. Leiomyosarcoma: computed tomographic findings. *Radiology.* 1984;152:133–136.
19. Nauert TC, Zornoza J, Ordonez N. Gastric leiomyosarcomas. *AJR Am J Roentgenol.* 1982;139:291–297.
20. Emory TS, Sobin LH, Lukes L, et al. Prognosis of gastrointestinal smooth-muscle (stromal) tumors: dependence on anatomic site. *Am J Surg Pathol.* 1999;23:82–87.
21. Cooper PN, Quirke P, Hardy GJ, et al. A flow cytometric, clinical, and histologic study of stromal neoplasms of the gastrointestinal tract. *Am J Surg Pathol.* 1992;16:163–170.
22. Koga H, Ochiai A, Nakanishi Y, et al. Re-evaluation of prognostic factors in gastric leiomyosarcoma. *Am J Gastroenterol.* 1995;90:1307–1312.
23. Cunnungham RE, Federspiel BH, McCarthy WF, et al. Predicting prognosis of gastrointestinal smooth muscle tumors. Role of clinical and histologic evaluation, flow cytometry, and image cytometry. *Am J Surg Pathol.* 1993;17:588–594.
24. Lerma E, Oliva E, Tugues D, et al. Stromal tumours of the gastrointestinal tract: a clinicopathological and ploidy analysis of 33 cases. *Virchows Arch.* 1994;424:19–24.

Primary Dedifferentiated Liposarcoma of the Retroperitoneum

Prognostic Significance of Computed Tomography and Magnetic Resonance Imaging Features

Ukihide Tateishi, MD, PhD, Tadashi Hasegawa, MD, PhD, Yasuo Beppu, MD, Mitsuo Satake, MD, and Noriyuki Moriyama, MD, PhD

Objectives: To describe computed tomography (CT) and magnetic resonance (MR) imaging findings and to determine the prognostic significance of radiologic appearances in primary dedifferentiated liposarcoma of the retroperitoneum.

Methods: Initial CT and MR imaging studies of 20 pathologically confirmed cases of primary dedifferentiated liposarcoma of the retroperitoneum were retrospectively reviewed and assessed for correlations with the histopathologic features. CT and MR images were evaluated by 2 radiologists with agreement by consensus, and univariate analyses were conducted to evaluate survival with a mean clinical follow-up duration of 47 months (range, 5–114 months).

Results: Tumor invasion was more frequent in the anterior or posterior pararenal originating tumors than in pararenal tumors ($P < 0.05$). Well-defined nonlipomatous masses juxtaposed with fatty tumors were identified in all cases. Calcification or ossification was seen in 6 patients (30%) on unenhanced CT. Imaging findings including attenuation, signal characteristics, and enhancement patterns of nonlipomatous masses were nonspecific regardless of histologic variances. Recurrent tumors (n = 6) tended to invade surrounding organs. Univariate analysis revealed that calcification or ossification ($P < 0.05$) and first recurrence with duration of a mean 13 months ($P < 0.05$) identified by imaging studies had significant impacts on overall survival.

Conclusions: Calcification or ossification and first recurrence identified by CT and MR imaging studies are significant adverse prognostic factors in primary dedifferentiated liposarcoma of the retroperitoneum.

From the Divisions of Diagnostic Radiology (Drs Tateishi, Satake, and Moriyama), Pathology (Dr Hasegawa), and Orthopedics (Dr Beppu), National Cancer Center Hospital and Research Institute, Tokyo, Japan.

This work was carried out by the Program for Promotion of Fundamental Studies in Health Sciences of the Organization for Pharmaceutical Safety and Research (Japan) and was supported in part by a Grant-in-Aid for Cancer Research from the Ministry of Health, Labor and Welfare (Japan).

Reprints: Ukihide Tateishi, MD, PhD, Division of Diagnostic Radiology, National Cancer Center Hospital, 5-1-1, Tsukiji, Chuo-Ku, Tokyo 104-0045, Japan (e-mail: utateish@ncc.go.jp).

Key Words: computed tomography, dedifferentiated liposarcoma, liposarcoma, magnetic resonance imaging

(*J Comput Assist Tomogr* 2003;27:799–804)

Liposarcoma is one of the most common soft tissue sarcomas. Tumors are currently classified into 3 groups: well differentiated liposarcoma (WDL) with or without dedifferentiation (DD), myxoid and round cell/cellular myxoid liposarcoma, and pleomorphic liposarcoma.[1] Dedifferentiated liposarcoma (DDL) was originally defined as the existence of a high-grade, nonlipogenic sarcoma juxtaposed to a WDL.[1,2]

It is now known that substantial areas of DD show a variety of histologic appearances, such as myxofibrosarcoma (myxoid malignant fibrous histiocytoma) and low-grade spindle-cell sarcoma.[3,4] Divergent differentiation often occurs within the DD areas in the form of osteosarcoma, leiomyosarcoma, or rhabdomyosarcoma.[5] WDL with almost entirely low-grade DD areas in the absence of high-grade DD areas, as well as a peculiar neural-like whirling pattern of DD, have previously been described.[6] This morphologic variability may lead to nonspecific and various computed tomography (CT) and magnetic resonance (MR) imaging features. The radiologic appearance of DDL reflects histologic coexistence of nonlipomatous mass and a predominantly fatty tumor. This bimorphic type of appearance is commonly seen in large tumors in the retroperitoneum.[7,8]

DDL behaves aggressively with a local recurrence rate of 41%, a metastasis rate of 17%, and a disease-related mortality of 28%.[5] However, little is known about the relationships between imaging features and prognosis. The purpose of our study was to define the CT and MR imaging characteristics of primary dedifferentiated liposarcoma of the retroperitoneum, with emphasis on imaging features affecting prognosis.

MATERIALS AND METHODS

We retrospectively reviewed 20 cases of DDL in the abdomen, which were registered in the pathology files of our in-

stitute. The clinical details, including follow-up information, were obtained by reviewing all the medical charts. Our institutional review board does not require its approval or patient informed consent for this type of review. Fourteen patients were male (70%) and 6 were female (30%). Their mean age at diagnosis was 59 years and ranged from 32 to 79 years. No patients were lost to follow-up, which began on the date of primary surgery. The median duration of follow-up was 47 months and ranged from 8 to 114 months.

Images reviewed included CT scans (in 20 patients; all with pre- and postcontrast enhancement) and MR images (in 20 patients with contrast enhancement). CT scan was performed with 1 of 2 models in all patients (Aquilion multislice CT scanner or X-Vigor, Toshiba Medical Systems, Tokyo, Japan). Scanning parameters were axial single- or 4-slice mode, 3.0–10.0-mm section thickness, 0.5–1.0 seconds/rotation, pitch 1:1–3, 120–150 kVp, and 200–250 mA. Images were reconstructed with 3.0-, 5.0-, and/or 10.0-mm slice thickness using a standard algorithm without edge enhancement. MR imaging was performed using 1 of 2 models of 1.5-T systems (General Electric Medical Systems, Milwaukee, WI, or Toshiba Medical Systems, Tokyo, Japan). Using the spin-echo or fast spin-echo technique, T1-weighted images (460–720/12–27 milliseconds [TR/TE]) were obtained in the transverse plane. T2-weighted images (3500–12000/80–112 milliseconds [TR/TE_{eff}]; 8–12 echo train) were then obtained in transverse and coronal planes using the body coil. The images were obtained with a field of view of 32–40 cm, an image matrix of 128 × 128–256, and a slice thickness of 6–10 mm. Gadopentetate dimeglumine was administered intravenously, and T1-weighted images were obtained in transverse and coronal planes with fat suppression.

Two radiologists reviewed the MR images, and the findings were reported by means of consensus. Radiologic findings assessed included location, tumor size, types of contours and margins, septal structure, tumor capsule, intralesional calcification or ossification, signal characteristics on T1- and T2-weighted images, and homogeneity (homogeneous or heterogeneous). Tumor location was determined by mainly affected sites of retroperitoneum; the pararenal space, and the anterior or posterior pararenal space. The signal characteristics were described as isointense or hyperintense relative to the signal intensity of skeletal muscle. Lesions containing areas with densities on CT or signal characteristics on T1- and T2-weighted MR images similar to those of subcutaneous fat were considered fatty components. The characteristics of fatty and nonliponmatous components or masses were categorized.

Histologic slides of all the tumors that were reviewed were in the patient files of the National Cancer Center Hospital. DD was defined as highly cellular areas with either a high mitotic rate (>5/10 high-power fields [HPF]) or marked pleomorphism, distinguishing these areas from the sclerosing type of WDL. Whenever necessary, immunohistochemical staining was carried out to confirm the diagnosis or tumor type according to the classification system. In all cases, representative sections from paraffin blocks of the primary or recurrent tumor with both WD and DD areas were examined. Tumors are divided according to the proportion of DD areas within the entire tumor: more than 50% or less. In this study, the histologic grade of a tumor was determined using a grading system.[9–11] The histologic grades were assigned as the highest grade present throughout the case.

Statistical Analysis

The demographics and imaging characteristics of the patients were compared using the Wilcoxon rank sum test for continuous variables and the χ^2 or Fisher exact test probability tests for categorized variables. Survival from the first operation until death caused by the tumor was assessed by the Kaplan-Meier method. Univariate analysis was performed by comparing Kaplan-Meier survival curves and carrying out log-rank tests. All analyses were conducted using SPSS software (version 11.0J; SPSS, Chicago, IL). Differences and correlations at a P value of <0.05 were considered to be statistically significant.

RESULTS

Clinical Findings

All tumors had DD areas initially (de novo) in the retroperitoneum. The mean tumor size was 19.3 cm (standard deviation [SD], 2.6 cm; range, 2.0–51.0 cm). The primary treatment was marginal excision at best in all cases. Excision of the tumors involved extensive surgical procedures, including total or partial removal of the kidney, adrenal gland, pancreas, colon, or spleen. Surgical treatment was followed by radiation therapy in 2 patients. Seven patients (35%) developed local recurrences; the period between primary excision and diagnosis of first recurrence ranged from 4 to 19 months (mean, 13 months). Most patients had multiple recurrences; in particular, 5 recurrences occurred in 1 patient over 6 years. Distant metastasis to lymph node or soft tissue was seen in 2 patients (10%).

Imaging Features and Prognosis

Tumor sites included the anterior paraspace in 7 patients (Fig. 1), pararenal space in 5 (Fig. 2), and posterior pararenal space in 8 (Fig. 3). Tumor invasion depicted on CT and MR imaging studies included the colon (n = 4), diaphragm or abdominal wall (n = 3), kidney (n = 2), small intestine or mesentery (n = 2), pancreas (n = 2), stomach (n = 1), ureter (n = 1), and inferior vena cava (n = 1). Tumor invasion was more frequent in anterior pararenal (57%) or posterior pararenal (50%) tumors than in pararenal (0%) tumors ($P < 0.05$) (Figs. 1, 3).

Eighteen tumors (90%) showed lobulated morphology. Two tumors (10%) were situated across the midline. Well-

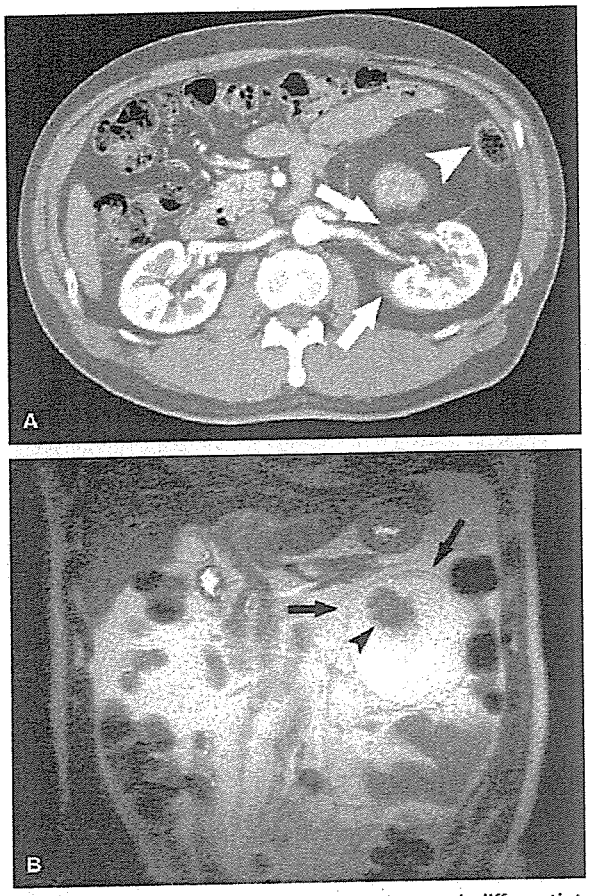

FIGURE 1. A 51-year-old man with primary dedifferentiated liposarcoma arising from the anterior pararenal space. A, Transverse enhanced CT image shows nonlipomatous masses abruptly juxtaposed with fatty tumor in the anterior pararenal space. Note the tumor juxtaposed with the descending colon (arrowhead) and the renal capsule and parapelvis (arrows). B, Tumor shows irregular contours with large amount of fat signal with capsule (arrows) on coronal T2-weighted fast spin-echo (TR/TE, 12000/80 milliseconds) MR image. Dedifferentiated (DD) areas (arrowhead) within the tumor were isointense relative to muscle of the abdominal wall.

defined nonlipomatous masses abruptly juxtaposed with fatty tumors (Fig. 1) were identified in 16 cases (80%) while 4 tumors (20%) showed blending transitions between nonlipomatous masses and fatty tumors. All nonlipomatous masses corresponded to DD areas on microscopy. DD areas accounted for more than 50% of the entire tumor in 12 tumors (60%). Septal structures (Fig. 2) were identified in 18 (90%). On T2-weighted MR images, the signal intensities relative to the muscle intensity of septal structures were low, and on contrast-enhanced MR images the septa were enhanced homogeneously. Microscopic examination revealed that the septal structures corresponded to fibrous bands containing collagen fibrils of varying thickness in which were embedded scattered spindle and multipolar stromal cells with hyperchromatic nuclei. Contrast-enhanced MR images revealed that all tumors (100%) had homogeneously enhanced tumor capsules (Fig. 1). All calcification (Fig. 2) or ossification (n = 6) on CT corresponded to pathologic metaplasia of 3 tumor types: fibrosarcoma, myofibrosarcoma, and mixed type. Ossification derived from osteosarcomatous or chondrosarcomatous element was seen in 1 patient. On T1-weighted MR images, the signals relative to those of muscle were hypointense (n = 14), isointense (n = 1), and hyperintense (n = 5) whereas on T2-weighted MR images, the tumors showed heterogeneous hyperintense (n = 20) signals relative to the muscle intensities. High-intensity

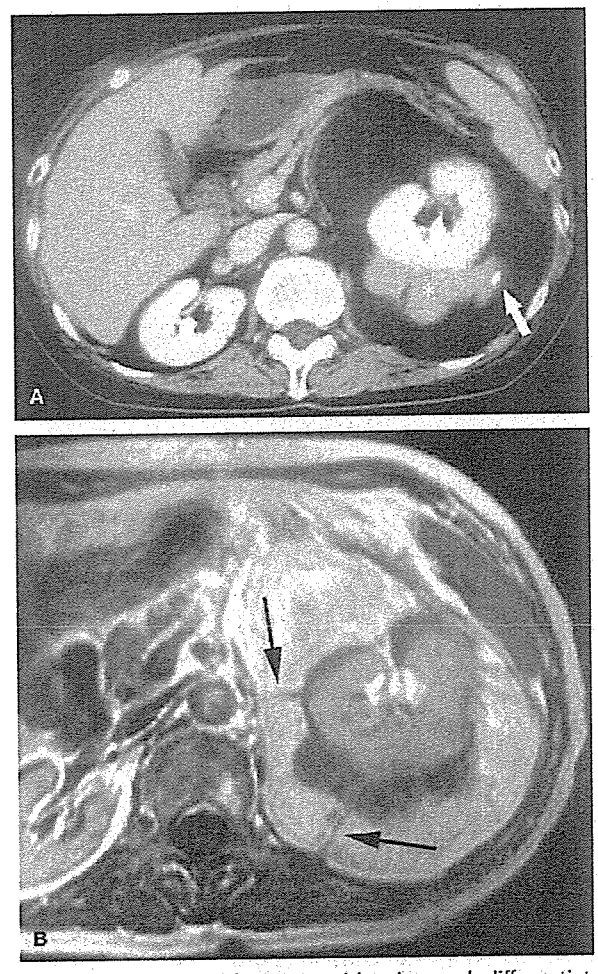

FIGURE 2. A 73-year-old woman with primary dedifferentiated liposarcoma arising from the pararenal space. A, Transverse enhanced CT image shows well defined nonlipomatous masses juxtaposed with fatty tumor in the pararenal space. Calcification (arrow) is noted within the DD areas (*). B, Transverse T2-weighted fast spin-echo (4000/82.5) MR image demonstrates septal structures within fatty tumor (arrows).

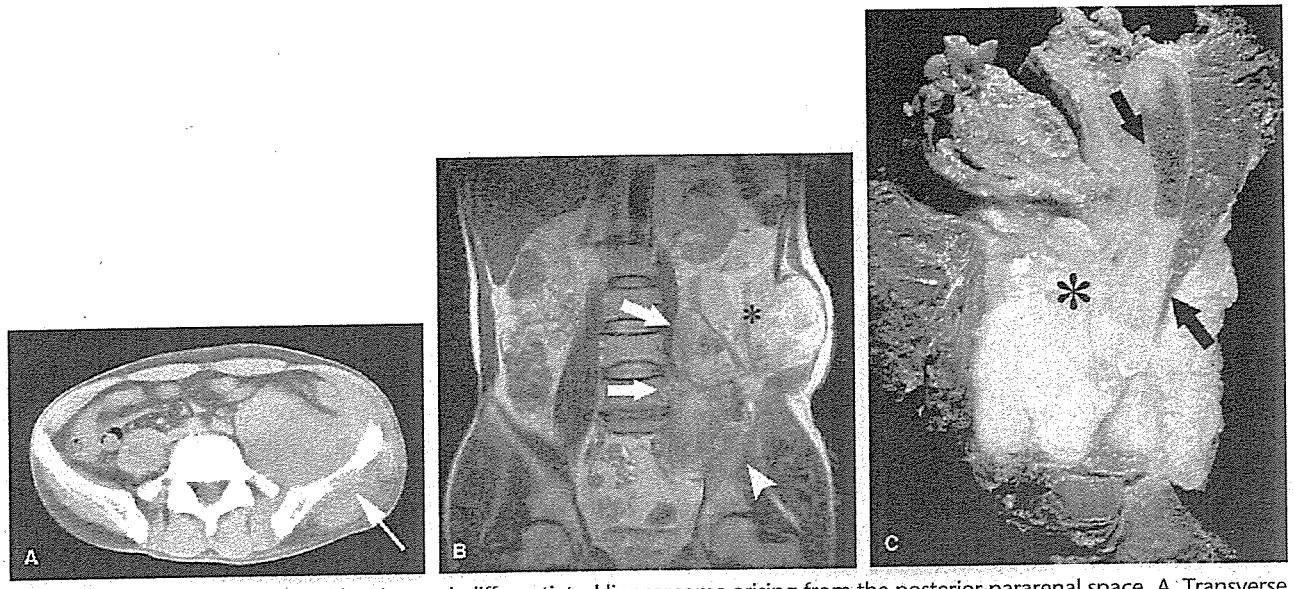

FIGURE 3. A 40-year-old man with primary dedifferentiated liposarcoma arising from the posterior pararenal space. A, Transverse enhanced CT image shows an irregular mass involving the abdominal wall and iliac bone (arrow). B, Tumor (*) extended laterally into abdominal wall, medially into the paraspinal region (arrows), and inferiorly in the pelvis (arrowheads) on coronal T2-weighted fast spin-echo (4000/82.5) MR image. C, Photograph of a macroscopic specimen shows tumor invasion (*) of the surrounding iliac bone (arrows), muscle, fascia, and subcutaneous tissue.

signals identified on both T1- and T2-weighted MR images were considered to be tumor hemorrhage in 2 tumors (25%). However, this signal pattern was also consistent with the presence of immature fatty tissue or fat components of tumor and various amounts of myxoid matrix or hyaluronic acid, which were observed under the microscope. Degenerated cysts confirmed by microscopy were identified in 1 patient (5%) on MR images. Imaging findings including attenuation, signal characteristics, and enhancement patterns of nonlipomatous masses were nonspecific regardless of histologic variances. The most common histologic patterns of nonlipomatous tumor included malignant fibrous histiocytoma (n = 5), myofibrosarcoma (n = 3), fibrosarcoma (n = 3), or myxofibrosarcoma (n = 2). Six tumors showed a combination of myxoid, spindle cell, and pleomorphic features (mixed type). One tumor showed predominantly neural-like whorls composed of ovoid to spindle cells with plump vesicular nuclei. All recurrent tumors (n = 6) showed irregular contours without containing an obvious fat component on CT and MR images. Recurrent tumors tended to invade the surrounding organs: colon (n = 2), diaphragm (n = 1), pancreas (n = 1), and small intestine (n = 1). Distant metastases were identified in 2 patients: inguinal nodal metastasis (n = 1) and subcutaneous soft tissue metastasis (n = 1). At the last follow-up, 17 patients (85%) were alive with or without disease and 3 (15%) had died of tumor. The estimated cumulative 5-year survival rate was 80%. The univariate analysis showed that calcification or ossification ($P < 0.05$) had a significant impact on overall survival (Fig. 4). Of 6 patients possessing tumors with calcification or ossification, 3 had high-grade nonlipomatous elements. These patients developed recurrent tumor and died of the disease with a mean duration of 13 and 52 months, respectively. In 6 patients who developed local recurrences, those with occurrence of the first recurrence (less

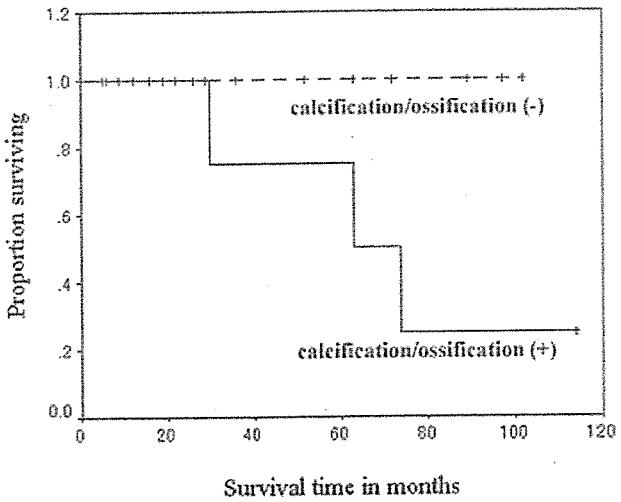

FIGURE 4. Kaplan-Meier survival curves for calcification or ossification in primary dedifferentiated liposarcoma of the retroperitoneum. The difference between 2 groups was statistically significant by log-rank test ($P < 0.05$).

than a mean of 13 months) identified on CT and MR images had significantly shorter survival than those without recurrences ($P < 0.05$) (Fig. 5). No other categorized variables, including age, sex, size, imaging features (ie, tumor location, types of contours, the presence of invasion, septal structure, or capsule, signal characteristics on T1- and T2-weighted images, and homogeneity), amount of DD, transition types, histologic subtype, and treatment, were correlated with survival.

DISCUSSION

In the current study, we have the documented radiologic appearances of retroperitoneal DDLs. The retroperitoneum represents the most common anatomic location for this lesion, outnumbering the soft tissues of the extremities.[1,2] The most important prognostic factor was anatomic location, with retroperitoneal lesions exhibiting the worst clinical behavior.[1–3] In the retroperitoneum, it is commonly impossible to obtain a wide surgical excision margin. In such cases, local recurrence is almost inevitable and often leads to death. Therefore, almost all retroperitoneal DDLs seem to recur locally if the patients are followed.[3] Our results showed similarly that the occurrence of the first recurrence with a mean duration of 13 months identified on CT and MR images was an adverse prognostic factor in univariate analysis.

The retroperitoneal DDLs in our study showed an aggressive clinical course with fatal outcome in 15% of cases and local recurrences in 30%. Although tumor size has previously been found to be prognostically significant, there was no relationship between tumor size and clinical course in our study.[12]

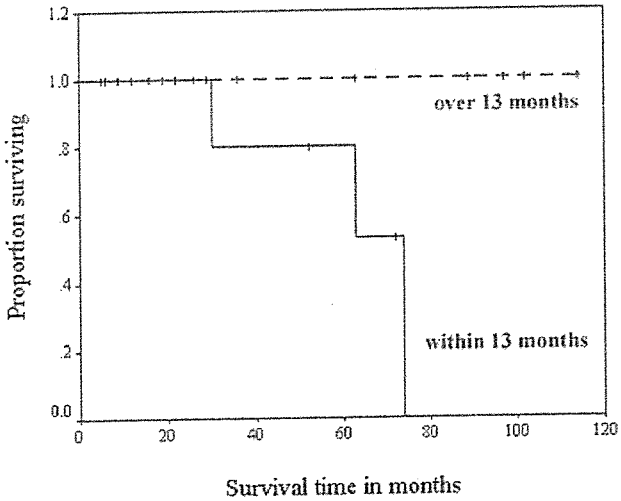

FIGURE 5. Kaplan-Meier survival curves for the first recurrence within 13 months or over 13 months in primary dedifferentiated liposarcoma of the retroperitoneum. The difference between 2 groups was statistically significant by log-rank test ($P < 0.05$).

The period to first recurrence was also correlated with clinical aggressiveness in recurrent cases, which seems attributable to the histologic diversity of DD areas. As most tumors displayed a varied histology, with myxoid, spindle cell, and pleomorphic regions in a given tumor, the lesion should be graded by the least-differentiated region.

A fatty mass with internal thick or thin septa has been identified in WDL on MR imaging.[13] London et al noted that septal structures on MR imaging studies were highly suggestive of a better-differentiated fatty component within the tumor.[14] The imaging characteristics of lipomatous areas were similar to WDL in our study. Septal structures, which were seen in 90% of our cases, corresponded to fibrous bands containing collagen fibrils of varying thickness on microscopic observation. The nonlipomatous areas appear as thickened, irregular septa or minor nodular components rather than as juxtaposed masses. Statistically significant features to predict WDL are male sex, presence of thick septa, and associated nonlipomatous masses.[13] The imaging findings of our DDL cases contained septal structures and nonlipomatous areas, which were in accordance with the imaging features of WDL.

CT and MR imaging studies revealed suggestive findings of DDLs: well defined nonlipomatous mass juxtaposed with a predominantly fatty tumor.[7,8] Most of our cases were in accordance with the previous results, but these findings did not assist the diagnosis in several tumors. There may be some reasons for this discrepancy. First, these findings may depend on the proportions of nonlipomatous and fatty elements and may be more nonspecific to tumors with large amounts of nonlipomatous mass. Although MR imaging is sensitive enough to detect minute fat deposits or immature fatty components, a tumor may contain various amounts of myxoid matrix composed of hyaluronic acid, which often shows similar signal intensity to that of fatty tissue on MR image, and this may affect diagnosis.[1–3] Second, 20% of our cases demonstrated a blending transition at the boundary between the nonlipomatous mass and fatty tumor, possibly rendering delineation of the tumor radiologically unclear. Finally, other histologic subtypes of liposarcoma appear to have less than 25% fat radiologically.[15] Other types of liposarcoma will have the potential to demonstrate similar findings.

In this study, the DD areas in 20 cases of DDLs showed a more varied histologic appearance than has previously been reported. The most common pattern was fibrosarcoma or malignant fibrous histiocytoma (MFH) (n = 8) followed by mixed type (n = 6), myofibrosarcoma (n = 3), and whorl structure (n = 1). DDL may exhibit heterologous differentiation in about 10% of cases. The most frequent lines of heterologous differentiation include osteo/chondrosarcomatous elements. A peculiar neural-like or meningothelial-like whorling pattern of dedifferentiation was also found in 1 of our cases. Interestingly, these patterns of dedifferentiation are often associated with ossification.[6] On unenhanced CT, 25% of 20 tumors ex-

hibited calcification or ossification which corresponded to metaplastic patterns of dedifferentiation in our study. MR imaging studies showed ossification consistent with signal voids and well defined fatty marrow.

Calcification or ossification is a distinct imaging pattern of DDL. These features are suggestive of metaplasia and often associated with meningothelial-like or neural-like whorls in DDL. In addition, we observed a single case with divergent osseosarcomatous or chodrosarcomatous differentation as reported in the prior studies.[16] Unexceptionally, the presence of calcification or ossification on unenhanced CT indicates metaplasia or differentiation within tumor in DDL. The relationship between prognosis and presence of metaplasia is not fully understood.[17–19] Although univariate analysis revealed that the calcification or ossification had a significant impact on overall survival, this was mainly because of the patient population. Of 6 patients with calcified metaplasia, 3 patients developed recurrent tumor and died of the disease with a short duration.

In summary, there is a spectrum of CT and MR imaging findings in retroperitoneal DDLs. The occurrence of the first recurrence identified on CT and MR images may be a predictor of adverse prognosis.

REFERENCES

1. Enzinger FM, Weiss SW. *Soft Tissue Tumors.* 4th ed. St Louis, MO: Mosby-Year Book, 2001.
2. Weiss SW, Rao VK. Well-differentiated liposarcoma (atypical lipoma) of deep soft tissue of the extremities, retroperitoneum, and miscellaneous sites: a follow-up study of 92 cases with analysis of the incidence of "dedifferentiation." *Am J Surg Pathol.* 1992;16:1051–1058.
3. Hasegawa T, Seki K, Hasegawa F, et al. Dedifferentiated liposarcoma of retroperitoneum and mesentery: varied growth patterns and histological grades. A clinicaopathologic study of 32 cases. *Hum Pathol.* 2000;31: 717–727.
4. McCormick D, Mentzel T, Beham A, et al. Dedifferentiated liposarcoma: clinicopathologic analysis of 32 cases suggesting a better prognostic subgroup among pleomorphic sarcomas. *Am J Surg Pathol.* 1994;18:1213–1223.
5. Henricks WH, Chu YC, Goldblum JR, et al. Dedifferentiated liposarcoma: a clinicopathological analysis of 155 cases with a proposal for an expanded definition of dedifferentiation. *Am J Surg Pathol.* 1997;21:271–281.
6. Nascimento AG, Kurtin PJ, Guillou L, et al. Dedifferentiated liposarcoma: a report of nine cases with a peculiar neurallike whirling pattern associated with metaplastic bone formation. *Am J Surg Pathol.* 1998;22: 945–955.
7. Munk PL, Lee MJ, Janzen DL, et al. Lipoma and liposarcoma: evaluation using CT and MR imaging. *AJR Am J Roentgenol.* 1997;169:589–594.
8. Kransdorf MJ, Meis JM, Jelinek JS. Dediffrentiated liposarcoma of the extremities: imaging findings in four patients. *AJR Am J Roentgenol.* 1993;161:127–130.
9. Hasegawa T, Yokoyama R, Lee YH, et al. Prognostic relevance of a histological grading system using MIB-1 for adult soft-tissue sarcoma. *Oncology.* 2000;58:66–74.
10. Hasegawa T, Yamamoto S, Yokoyama R, et al. Prognostic significance of grading and staging systems using MIB-1 score in adult patients with soft tissue sarcoma of the extremities and trunk. *Cancer.* 2002;95:843–851.
11. Hasegawa T, Yamamoto S, Nojima T, et al. Validity and reproducibility of histologic diagnosis and grading for adult soft-tissue sarcomas. *Hum Pathol.* 2002;33:111–115.
12. Elgar F, Goldblum JR. Well-differentiated liposarcoma of the retroperitoneum: a clinicopathologic analysis of 20 cases, with particular attention to the extent of low-grade dedifferentiation. *Mod Pathol.* 1997;10:113–120.
13. Kransdorf MJ, Bancroft LW, Peterson JJ, et al. Imaging of fatty tumors: distinction of lipoma and well-differentiated liposarcoma. *Radiology.* 2002;224:99–104.
14. London J, Kim EE, Wallace S, et al. MR imaging of liposarcomas: correlation of MR features and histology. *J Comput Assist Tomogr.* 1989;15: 832–835.
15. Jelinek JS, Kransdorf MJ, Shmookler BM, et al. Liposarcoma of the extremities: MR and CT findings in the histologic subtypes. *Radiology.* 1993;186:455–459.
16. Orui H, Ishikawa A, Tsuchiya T, et al. Chondro-osseous differentiation in fat tissue tumors: magnetic resonance imaging with pathologic correlation. *Skeletal Radiol.* 2000;29:459–465.
17. Lucas DR, Nescimento AG, Sanjay BKS, et al. Well-differentiated liposarcoma: the Mayo clinic experience with 58 cases. *Am J Clin Pathol.* 1994;102:677–683.
18. Orson GG, Sim FH, Reiman HM, et al. Liposarcoma of the musculoskeletal system. *Cancer.* 1987;60:362–370.
19. Reitan JB, Kaazhus O, Brenhoud IO, et al. Prognostic factors in liposarcoma. *Cancer.* 1985;55:2482–2490.